Unveiling the Domain-Specific and RAS Isoform-Specific Details of BRAF Regulation

Tarah Trebino[1], Borna Markusic[1,2], Haihan Nan[1,3], Shrhea Banerjee[1], Zhihong Wang[1,4]
[1]Rowan University, 201 Mullica Hill Rd, Glassboro, NJ 08028, USA
[2]Max Planck Institute of Biophysics, Max-von-Laue Straße 3, 60438 Frankfurt am Main, Germany
[3]School of Laboratory Medicine and Life Science, Wenzhou Medical University, Wenzhou, Zhejiang, 325035, China
[4]corresponding author (wangz@rowan.edu)

Abstract

BRAF is a key member in the MAPK signaling pathway essential for cell growth, proliferation, and differentiation. Dysregulation or mutation of BRAF is often the underlying cause of various types of cancer. RAS, a small GTPase protein that acts upstream of BRAF, has been identified as a driver of up to one-third of all cancers. When BRAF interacts with RAS via the RAS binding domain (RBD) and membrane recruitment, BRAF undergoes a conformational change from an inactive, autoinhibited monomer to an active dimer and subsequently phosphorylates MEK to propagate the signal. BRAF domains are involved in specific functions of the regulatory mechanism, as exampled by maintenance of the autoinhibited conformation through interactions between the Cysteine Rich Domain (CRD) and the Kinase Domain (KD) of BRAF. Despite the central role of BRAF in cellular signaling, the exact order and magnitude of its activation steps has yet to be confirmed experimentally. We employed pulldown assays, open surface plasmon resonance (OpenSPR), and hydrogen-deuterium exchange mass spectrometry (HDX-MS) to investigate the roles of the regulatory regions in BRAF activation and autoinhibition. Our results demonstrate that the BRAF specific region (BSR) and CRD play a crucial role in regulating the activity of BRAF. Moreover, we quantified the autoinhibitory binding affinities between the N-terminal domains of BRAF and the KD and revealed the individual roles of the BRAF regulatory domains. Furthermore, we quantified the relief of autoinhibition between the N-terminal domains of BRAF and the KD upon RAS binding, providing direct evidence that RAS binding initiates RAF activation. Additionally, our findings provide evidence that the BSR negatively regulates BRAF activation in a RAS isoform-specific manner and highlight the importance of considering the specific isoform pairs when developing inhibitors targeting RAF-RAS interactions. Our findings also indicate that oncogenic BRAF-KD^{D594G} mutant has a lower affinity for the regulatory domains, implicating that pathogenic BRAF acts through decreased propensity for autoinhibition. Collectively, our study provides valuable insights into the activation mechanism of BRAF kinase and may help to guide the development of new therapeutic strategies for cancer treatment.

Keywords: BRAF, CRAF, KRAS, HRAS, RAS binding domain, cysteine rich domain, BRAF specific region, autoinhibition, domain-domain interactions

Abbreviations

RAF (Rapidly Accelerated Fibrosarcoma; isoforms A-, B-, and C-); MAPK (Mitogen Activated Protein Kinase); RAS (Rat Sarcoma; isoforms H-, K-4a, K-4b, and N-); GTP (guanosine triphosphate); ATP (adenosine triphosphate); GAP (GTPase Activating Protein); GEF (Guanine Exchange Factor); MEK (MAPK/Erk Kinase); ERK (Extracellular signal-regulated kinase); BSR (BRAF specific region); RBD (RAS Binding Domain); CRD (Cysteine Rich Domain); CR1 (Conserved Region 1); CR2 (Conserved Region 2); CR3 (Conserved Region 3); KD (Kinase Domain)

Introduction

The RAF family, composed of A-, B-, and CRAF (Raf1) in mammalian cells, are serine/threonine kinases that function to modulate cell growth and differentiation.[1] The RAF family is a key component in the RAS-RAF-MEK-ERK (MAPK) signaling cascade. Upon extracellular stimulation, the GTPase protein, RAS, becomes activated with the aid of GEFs to adopt the GTP-bound active form.[2] Subsequently, RAF is activated by a number of events such as: interacting with active RAS,[3,4] relieving autoinhibition,[5,6] translocating to the membrane, and forming dimers.[7] Active RAF then phosphorylates and activates MEK, which in turn phosphorylates and activates ERK.[8] Finally, activated ERK translocates to the nucleus, where it regulates various cell processes.[9] A significant number of cancers are linked to mutations of MAPK components, with RAS being mutated in 10-30% of all human cancers.[10] BRAF mutations are the cause of roughly 8% of cancers.[11] In addition, germline mutations in RAS and RAF lead to RASopathies—a variety of genetic diseases that cause developmental disorders such as facial deformation and cardiovascular deficiencies.[12]

Targeting RAS in cancer treatments is challenging because of its compact shape, shallow cavities on its smooth surface, and extremely high binding affinity for GTP. Currently, despite decades of research, RAS only has two FDA-approved inhibitors that work by covalently attaching to the oncogenic G12C mutation of KRAS.[13,14] RAS has four isoforms (NRAS, HRAS, KRAS4A, and KRAS4B) and numerous common oncogenic mutations other than the G12C mutation. Furthermore, BRAF mutations are categorized into 3 classes based on RAS- and dimer-dependency.[15] The most common BRAF mutation is the V600E substitution, a class 1 RAS- and dimer-independent mutation.[11] Class 2 mutants are RAS-independent but dimer-dependent and class 3 mutants are both RAS- and dimer-dependent.[15] However, FDA-approved inhibitors, vemurafenib, dabrafenib, and encorafenib, are limited to class 1 mutations due to relief of negative feedback pathways and paradoxical activation phenomenon observed in class 2 and 3 mutants.[15–17] These limitations arise from knowledge gaps in RAF regulation and shortcomings in current drug treatments. Therefore, elucidating the details of the RAS-RAF interaction and the regulatory events surrounding it are essential for advancing the field and designing new therapies for the biological system that is prevalent in human cancers.

The RAF kinase family is comprised of three main conserved regions (CR1, CR2, and CR3), each with specific, non-overlapping functions in RAF regulation (Figure 1). The CR1 contains the RAS binding domain (RBD) and the cysteine rich domain (CRD). The CR2 is a flexible linker region that harbors a RAF phosphorylation and binding site for 14-3-3, which helps maintain RAF in its autoinhibited state.[18] The CR3 contains the catalytic or kinase domain (KD), which is important for RAF dimerization and phosphorylation of MEK substrates.[7,19] The N-terminal region, also known as the regulatory region, is an essential feature of RAF

architecture which regulates RAF activity through the concerted actions of the domains in this region: the RBD, CRD, and BRAF specific region (BSR) in BRAF.

The CRD has multifaceted roles in membrane recruitment, RAS interaction, as well as RAF autoinhibition. RBD-CRD interactions with RAS and direct interaction with anionic phospholipids anchor RAF to the membrane for RAF activation.[20–23] While the RBD is the primary domain involved in the strong nano-molar affinity interaction with RAS, a number of studies have also shown that the CRD increases the affinity of CRAF for HRAS, even though the CRD has a weaker micromolar affinity on its own.[24–26] Early research showed that CRD interaction with RAS is required for RAF activation.[20,25] Recently, the crystal structure of KRAS with CRAF-RBD-CRD revealed the CRD binding interface interactions at the interswitch region and C-terminal helix α5 of KRAS and solidified the necessity of the CRD-RAS interaction for RAF activation through mutagenesis experiments.[27] Another structure of the CRAF-RBD-CRD with HRAS, resolved nearly concurrently, also supported the centrality of the CRD, in which it is poised to modulate RAS and RAF functionalities because of its location at the base of two RAS protomers.[28] The cryo-EM structures of autoinhibited BRAF in complex with the regulatory protein 14-3-3 and MEK also confirmed the importance of the CRD in negatively regulating catalytic activity through contacts with the BRAF C-terminal kinase domain (KD) and 14-3-3.[18,29] CRD-KD interactions stabilize the inactive monomeric complex and 14-3-3 blocks the BRAF dimer interface and thereby activation of the kinase domains.[18] By combining their structure results with simulations, a mechanism was proposed: extraction of the CRD through RAS interaction leads to activation of RAF.[27,29] Additionally, the RBD is suggested to be a critical modulator of the transition from monomeric to dimeric RAF complexes because of steric clash that would occur upon RAS binding.[29] However, none of the structural studies was able to capture the BSR, probably due to its high degree of flexibility.

Differences between RAF isoforms are an important and not yet fully understood distinction in MAPK activation. While many studies have examined the structure and regulation of CRAF, these findings may not translate to all RAF isoforms. BRAF has the highest basal activity compared to ARAF and CRAF and is thus mutated most frequently in cancer.[30,31] Furthermore, compared to CRAF-CRD, the BRAF-CRD exhibits increased autoinhibitory activity and membrane binding.[32] BRAF and CRAF are suggested to have different preferences for H/K/N-RAS, although discrepancy exists among these studies.[22,33] Compared to CRAF, BRAF associates with unmodified HRAS with much higher affinity.[22] However, in recent BRET studies, BRAF was shown to prefer KRAS over HRAS, whereas CRAF did not differentiate between RAS isoforms.[33] The BSR was implicated in regulating these distinct binding preferences with RAS isoforms.[33]. Other than this recent study, relatively little research has examined the role of the BSR despite being one of the most noticeable isoform differences, making it an intriguing feature of regulation to study.

The Raf activation process is dynamic and complex, and despite years of research many details remain unclear. While many of BRAF's activation steps are built upon static structures and cell-based site-directed mutagenesis, the order and magnitude of these events has yet to be experimentally validated *in vitro*. The precise mechanism of how autoinhibition is released upon RAS binding is unknown, as well as the communication between the regulatory domains and the kinase domain. Our knowledge of the RAS-RAF interaction is derived mainly through characterization of CRAF, and a comprehensive analysis of BRAF-RAS interaction is still missing. BRAF has long been believed to have a distinct regulation mechanism, however, it remains elusive how BRAF differentiates itself from other RAF family members.

Here we investigated the interactions of BRAF regulatory regions with the C-terminal KD and with upstream regulators, HRAS and KRAS. To our knowledge, we present the first reported K_D values for the N- and C-terminal interactions of BRAF. Our results demonstrate that the CRD plays a primary role in autoinhibitory interactions, while the presence of the BSR increases the affinity for the KD. The RBD is the primary driver of RAS-RAF binding, however the BSR and CRD have allosteric effects that slow the association with HRAS. We found that the BSR does not interact with HRAS but provides isoform specificity towards KRAS. We also show that HRAS binding to BRAF disrupts the N- to C-terminal autoinhibitory interactions and that the oncogenic $BRAF^{D594G}$ can relieve autoinhibition to promote activity. Overall, this comprehensive *in vitro* study of the BRAF N-terminal region provides new insights into BRAF regulation.

Results

Specific purified BRAF N-terminal domains are involved in interacting with HRAS

The interactions between RAS and RAF have been well established, occurring primarily between the RAF-RBD region and secondarily between the RAF-CRD region to enhance the affinity for RAS.[34] However, the contribution of each regulatory domain to the BRAF activation mechanism is still not completely understood. We hypothesized that studying the differences in HRAS binding to various BRAF N-terminal constructs (NTs) would highlight the role of each domain and their cooperation in finetuning BRAF activity. We purified four different N-terminal BRAF constructs comprising an N-terminal MBP tag and various domains: NT1 (aa 1-288), NT2 (aa 1-227), NT3 (aa 151-288), and NT4 (aa 151-227; Figure 1A&B). We also purified active GST-tagged, GMPPNP-loaded, full-length HRAS and inactive, GST-tagged, GDP-loaded, full-length HRAS. The GST-tag forces HRAS into a dimeric state to recapitulate the active physiological conditions, as verified by size exclusion chromatography (Supplementary Fig 1A). After incubating BRAF NT1 with either GMPPNP-HRAS or GDP-HRAS for 1h, we conducted pulldown assays, in which NT1 is captured by amylose beads and probed for HRAS. Our results demonstrate that GMPPNP-HRAS binds to BRAF NT1 with stronger affinity than inactive GDP-HRAS, confirming that the purified HRAS protein, both the active form and inactive form, behaves as expected (Figure 1B&C). We also found that all NT constructs bind to GMPPNP-HRAS in pulldown assays, suggesting that purified BRAF fragments *in vitro* recapitulate the physiological protein-protein interactions that occur in cells (Figure 1D).

HDX-MS revealed conformational changes of BRAF N-terminal domains in response to HRAS binding

To further evaluate the specific regions of interaction and conformational changes in the BRAF regulatory domain upon HRAS binding, we performed hydrogen-deuterium exchange mass spectrometry (HDX-MS) experiments with two constructs, NT2 (includes BSR and RBD) and NT3 (includes RBD and CRD). Both constructs were incubated with and without GMPPNP-HRAS in D_2O buffer for set labeling reaction times (NT3: 2 sec [NT3 ± HRAS only], 6 sec [NT3 ± HRAS only], 20 sec, 30 sec [NT3 ± HRAS only], 60 sec, 5 min, 10 min, 30 min, 90 min, 4.5 h, 15 h, and 24 h), injected through a pepsin column for digest, and analyzed for deuterium uptake through mass spectrometry. Of the two approaches that exist within the field, we followed the practice of performing exchange reactions across broad range of labeling time points (much more than four orders of magnitude) to assign data significance rather than multiple replicates of

a few time points. Both constructs have multiple overlapping peptides for almost all residues and good sequence coverage for NT2 and NT3 (Supplementary Fig 2). The resulting peptide plots display rate changes of deuterium uptake across the wide range of labeling time points of NT2 and NT3 in D_2O. Data are displayed as the uncorrected deuterium uptake (no back exchange corrections) since maximal labeling (100% D uptake) was not demonstrated for the control apo-proteins, in which labeling reactions were performed for 24 h at room temperature and quenched at pH 2.4. A trend of multiple overlapping peptides from multiple charge states within a sequence range was considered high confidence of whether binding of HRAS has occurred to either induce an increase or decrease in deuterium exchange.

Peptides from HDX-MS experiments with NT2 and HRAS have decreased deuterium uptake encompassing amino acids 174-188 of BRAF, indicating that residues in the RBD interact directly with HRAS (Figure 2A). Similar to the results obtained with NT2, peptides from experiments with NT3 and HRAS have decreased deuterium uptake in a broader region of amino acids 158-188, corresponding to most of the RBD (Figure 2A). Since the full-length structure of BRAF is still unresolved, we applied the AlphaFold Protein Structure Database for a model of BRAF to examine the conformation of the N-terminal domains and display the HDX-MS results.[35,36] The RBD domain of the BRAF model we employed (UNIPROT ID: P15056) overlays similarly to resolved structures of this region in complex with HRAS (PDB ID: 4G0N).[37] We mapped the change in deuterium uptake on the AlphaFold BRAF structure, with red regions indicating decreased deuterium uptake (protected region upon HRAS binding; Figure 2B&D). These regions of slower deuterium exchange lie within the expected binding interface of BRAF and include the critical Arg188 residue (R89 in CRAF) for RAS binding.[27,38] Our results are consistent with the current model that the RBD is the main region of interaction between BRAF and HRAS. These results further verified that the protein-protein interactions we captured here are physiologically relevant and that the proteins we purified from *E. coli* recapitulate the key elements of RAF regulation.

Peptides located outside of the RBD binding region do not display decreased deuterium uptake when HRAS is present (Figure 2A&C). Although a few peptides within the BRAF-CRD region show slower exchange from HDX-MS experiments with NT3 and HRAS, this phenomenon does not appear to occur in the majority of peptide fragments (Supplementary Fig 3). Therefore, we cannot conclusively demonstrate interactions with HRAS around the CRD region. However, this may be due to the reported micromolar affinity for the CRD domain's interaction, which is close to the detection limit for HDX-MS studies.[26]

Interestingly, we observed that peptides in the BSR region of NT2 exchange deuterium at a faster rate when bound to HRAS, indicating that HRAS binding induces exposure of the BSR to the environment (Figure 2A). The peptides with increased deuterium uptake correspond to BRAF residues 49-64, and while coverage of peptides corresponding to BRAF 82-99 is not as strong, this region also displays some acceleration of exchange (Figure 2A; Supplementary Fig 4). We denote the increased deuterium uptake on the AlphaFold BRAF structure with cyan regions (Figure 2B). The two alpha-helices of the BSR, predicted by AlphaFold, are the same regions where BRAF-NT2 residues are more exposed to the environment when bound to HRAS (Figure 2B). The BSR is thought to be a highly flexible domain, and the AlphaFold structure prediction has low confidence in the global orientation of the BSR compared to the other domains, therefore we cannot accurately determine the location of this domain within the HRAS:BRAF complex. Nonetheless, the observations that the BSR is more exposed upon HRAS

binding suggest the BSR might be less compatible with HRAS, and conformational changes in the N-terminal region occur in the presence of HRAS.

BRAF specific region (BSR) in conjunction with the cysteine rich domain (CRD) reduces binding affinity for HRAS

To further reveal the role of each domain, we measured the binding affinities of HRAS to each NT construct through OpenSPR experiments. In all experiments, we immobilized His-tagged NTs to a Ni-NTA sensor and flowed over HRAS in the OpenSPR with a flow rate of 30 μL/min. BRAF NT2, NT3, and NT4 bind to HRAS with nanomolar affinity (K_D=7.5 ± 3.5 nM, 22 ± 11 nM, and 19 ± 11 nM, respectively [average ± standard deviation]; Figure 3B-E). It is noteworthy that the K_D of NT2 from our study (K_D=7.5 nM) is similar to the previously reported K_D for BRAF residues 1-245 (BSR+RBD) purified from insect cells (K_D=11 nM).[22] Surprisingly, we were unable to observe binding with NT1 even under many varying conditions, changes in experimental design, and new protein preparations (Figure 3A). Since the interaction was captured by pulldowns (Figure 1D) but not OpenSPR, we investigated whether the interaction time is involved in this discrepancy. We therefore immobilized NT1 and flowed over HRAS at a much slower flow rate (5 μL/min), during which we saw minimal but consistent binding (Supplementary Fig 5A). The low response and long timeframe of each injection, however, makes the dissociation constant (K_D) unmeasurable and incomparable to our other NT-HRAS OpenSPR results. We propose that the conformation of the whole N-terminal region, when BSR, RBD, and CRD are together, prevents fast association with HRAS. Since truncated BRAF containing only BSR and RBD still binds with high affinity, the inclusion of the CRD in NT1 comprises the main binding differences. These results, together with HDX-MS, suggest that the BSR negatively regulates the interaction between HRAS and BRAF, likely in conjunction with the CRD, by blocking the RAS binding surface.

To further validate the slower association rate of BRAF NT1 to HRAS, we performed time-dependent competition pulldowns to compare the association rates of NT1 and NT3 to HRAS (Figure 3F). Initially, NT1 and HRAS were incubated for 1 h and followed by the subsequent addition of NT3 for 5, 15, and 30 min. We observed that after 15 min, NT3 started to associate with HRAS, which then proceeded with a time-dependent increase in association (Figure 3F). In contrast, when NT3 and HRAS were first incubated for 1 h, and then NT1 was subsequently added for 5, 15, and 30 min, NT1 did not show any association with HRAS (Figure 3G). Time-dependent pulldowns of HRAS and NT1 alone show that NT1 binds minimally within 5 min and reaches maximal binding by 30 min (Supplementary Fig 5B). These pulldown results are consistent with OpenSPR data and support that NT3 has a much faster and stronger association with HRAS and that NT1 is not able to outcompete NT3 for binding to HRAS.

BSR differentiates the BRAF-KRAS interaction from the BRAF-HRAS interaction

To validate our hypothesis that the BSR negatively regulates BRAF activation in a RAS isoform specific manner, we conducted experiments to investigate the interaction between BRAF and KRAS. We purified GST-tagged, dimeric full-length KRAS4b (Supplementary Fig 1B & C), which includes the C-terminal hypervariable region (HVR). The HVR is an important region for regulating RAS isoform differences, like membrane anchoring, localization, RAS dimerization, and RAF interactions.[39] Using OpenSPR, we observed that BRAF-NT1 binds active KRAS with a K_D of 265 ± 7 nM (Figure 4A), as opposed to HRAS, in which no binding was observed

(Figure 2A). In equivalent runs with KRAS and BRAF-NT2, we observed a K_D of 33 ± 5 nM (Figure 4B). Furthermore, through pulldowns in which KRAS was captured on glutathione resin and BRAF-NTs were probed, we observed that active KRAS binds to both BRAF-NT1 and NT2, whereas inactive KRAS does not (Figure 4C&D). These results, combined with HDX-MS results, which showed that the BSR is exposed when bound to HRAS, suggest that the electrostatic forces surrounding the BSR promote BRAF autoinhibition and the specificity of RAF-RAS interactions.

BSR and CRD promote BRAF autoinhibitory interactions

In addition to interacting with RAS, the BRAF N-terminal regulatory region is also important in maintaining the autoinhibited conformation.[5,40,41] Specifically, structures of autoinhibited BRAF in complex with MEK and 14-3-3 reveal that the CRD makes key interactions with the KD.[18,29] The BSR is not resolved in this structure, however, and much less is known about the roles of BSR and RBD in BRAF autoinhibition. To better understand the intra-domain interactions involved in BRAF autoinhibitory, we investigated the binding preferences of the four NT (NT1-4) constructs to the N-terminally 6xHis-tagged BRAF kinase domain (KD) purified from *E. coli.* We performed pulldown experiments with BRAF constructs NT1-4, in which biotinylated BRAF-KD was captured on streptavidin beads and probed for bound His/MBP-tagged BRAF NTs. Analysis through western blotting showed that NT1 and NT3 do indeed bind to KD, but NT2 and NT4 do not bind (Figure 5A). In accordance with the literature, these results show that the CRD is necessary and that BSR and RBD are not the primary contacts in autoinhibitory interactions with KD.

These results were further validated through OpenSPR experiments, which quantified the first *in vitro* binding affinity values for BRAF autoinhibition interactions. By immobilizing KD on a carboxyl sensor and flowing over increasing concentrations of NT1 (5, 15, 44, 133, 400 nM) at 30 µl/min, we observed specific binding between KD and NT1, with a K_D of 11 ± 1.5 nM (Figure 5B&C). An equivalent OpenSPR experiment with KD and NT3 produced a K_D of 54 ± 24 nM, higher than the dissociation constant between KD and NT1 (unpaired T-test $p < 0.05$; Figure 5B&D). The difference between NT1 and NT3 is the inclusion and exclusion of the BSR, respectively. This shows that the presence of the BSR increases the affinity for KD, further implicating that the BSR is important for stabilizing the autoinhibited state. The OpenSPR experiments with NT2 and NT4 showed very little specific binding even at higher concentrations of analyte (NT2: 1.125, 2.25, 4.5 µM; NT4: 1.5, 3, 6 µM; Figure 5E&D) with K_D values >4.5 µM (NT2) and >6 µM (NT4).

The RAS-RAF interaction directly disrupts RAF autoinhibition

Given the implication of RAS in relieving RAF autoinhibition, we performed pulldown experiments with HRAS, KD, and NT1 to investigate how RAS affects the association of the N- and C-terminal domains of BRAF. Specifically, GST-HRAS was captured on glutathione resin and probed for interactions between NT1 and KD. In this experiment, equal molar ratios of NT1 and KD were pre-incubated for 1 h to allow for binding, mimicking the autoinhibited monomeric BRAF. Then HRAS-bound resin was added, representing the activation event following RAS association. The pulldowns clearly showed that NT1 was associated with HRAS on the resin, while no KD was found in the fraction of NT1 that was bound to HRAS. These results demonstrate that KD is unable to bind to NT1 in the presence of HRAS (Figure 6A).

Our pulldown experiments were complemented with OpenSPR experiments. NT1 and HRAS were pre-incubated in equal molar amounts (400 nM for each) for 1 h, allowing for sufficient binding prior to injecting onto the KD-immobilized sensor. A comparison between binding of NT1 and KD with and without HRAS showed that the presence of HRAS abolished the interaction between NT1 and KD (Figure 6B). These findings demonstrate that HRAS binding to BRAF directly relieves BRAF autoinhibition by disrupting the NT1-KD interaction, providing the first *in vitro* evidence of RAS-mediated relief of RAF autoinhibition, the central dogma of RAS-RAF regulation.

Oncogenic BRAF-KD^{D594G} has decreased affinity for NT1 and thus attenuates autoinhibitory interactions

Although oncogenic mutations in BRAF are thought to relieve autoinhibitory interactions thereby promoting dimerization and activation, there is currently no direct evidence to support this hypothesis. To investigate this further, we purified the 33 kDa BRAF kinase domain with oncogenic mutation D594G (referred to as KD^{D594G}). BRAF^{D594G} is the most common BRAF mutant found in non-small cell lung cancer patients and has been identified as oncogenic despite the fact that its kinase activity is completely dead.[43] Previous studies have shown that the D594G mutant has higher dimerization potential than wild-type BRAF,[42] but it remains unclear how this mutation relieves the dimer interface from autoinhibitory interactions. To test our hypothesis that KD^{D594G} has lower autoinhibitory potential, we analyzed the binding affinity of NT1 and KD^{D594G} through OpenSPR and pulldown assays. We immobilized KD^{D594G} on a carboxyl sensor to the same response level as KD^{WT} (~6000 RU's) and flowed over the same concentrations of NT1 in both sets of experiments. With KD^{D594G}, we observed less binding to NT1 compared to KD^{WT}, and the responses were too low to calculate a K_D (Figure 6C). These results were validated using a pulldown experiment in which both KD proteins were biotinylated and pulled down on streptavidin beads. Binding of NT1 was subsequently probed through western blot (Figure 6D) and little to no NT1 was bound to KD^{D594G}, in direct contrast to KD^{WT}. These findings support our hypothesis that the D594G mutation significantly decreases the autoinhibitory interactions, rendering its oncogenic potential.

Discussion

In this study, we investigated the regulation of BRAF by examining the interactions between its N-terminal domain and RAS, as well as its C-terminal catalytic domain. Our findings, which were obtained from pulldowns, OpenSPR, and HDX-MS, suggest that the BSR in conjunction with the RBD and CRD inhibits HRAS binding by attenuating its ability to bind HRAS quickly. Additionally, we found that the NT1 construct, which includes the BSR, has the highest affinity for BRAF-KD, providing further direct evidence that these three domains fold into an autoinhibited conformation. The BRAF activation mechanism involves a nuanced set of events that is regulated by individual functions of the BRAF N-terminal domains in concert with the BRAF catalytic domain and RAS binding. We propose a mechanism for BRAF regulation: the BSR promotes RAF isoform-specific activity by maintaining autoinhibition, working in concert with the CRD, and encouraging KRAS association over HRAS. RAS binding to the RBD directly relieves BRAF autoinhibition, ultimately leading to activation (Figure 7).

RAS oncogenes are prominent drivers of human tumors, acting through effectors such as RAF and initiating over-activation of the MAPK pathway. The interaction between the RBD-CRD of RAF and the switch I and interswitch region of RAS has previously been established,[27] but the molecular mechanism behind RAF activation upon RAS binding is not fully understood. While a number of structural studies have recently emerged, a comprehensive analysis of the effects of RAS binding on BRAF relief of autoinhibition and activation is needed to design new therapies. Our *in vitro* analyses of the individual binding profiles of distinct regulatory regions of BRAF add to the growing body of evidence about BRAF activation. We isolated the three regulatory domains in BRAF to show their direct effects on RAS binding through quantitative K_D values. Since NT2, NT3, and NT4 have similar binding affinities for HRAS, our findings support that the RBD is the primary driver of the RAS-RAF interaction, as expected. The presence of the BSR clearly slows the ability for HRAS to bind, revealing a critical regulatory role for this region. Additionally, our results implicate the BSR as a potential target for further study to reinforce the conformation with the BSR and prevent BRAF activation through RAS interaction. SPR experiments from Tran *et al.* that examined the KRAS-CRAF interaction found that the presence of the CRD increases the binding affinity significantly.[27] The authors conclude that the CRD is important for differentiating between the RAS GTPase superfamily, even though high sequence homology exists between the switch-I region and the RBDs of RAF.[27] Interestingly, our results show that the CRD does not affect the affinity of BRAF towards HRAS, with binding affinity values within the same nanomolar range for constructs NT2-4. This could be due to RAF isoform differences, as slight amino acid differences are found in the sequence despite the conservation of the CRD in RAF kinases. Certain CRAF-CRD mutations that are key CRD-KRAS contacts were shown to increase the K_D values of binding to KRAS.[27] The mutation with the most prominent difference, K179, corresponds with sequence divergence between B- and C-RAF. While KRAS and HRAS are identical in the interswitch region, these RAF differences may provide an additional layer of regulation in RAS-mediated activation.

RAS isoforms are believed to have distinct impacts on effector binding and activation. Although these isoforms are highly conserved, the C-terminal hypervariable region (HVR) distinguishes HRAS from KRAS in significant ways. Cell-based assays suggest that KRAS recruits and activates CRAF more efficiently than HRAS,[44] whereas *in vitro* binding studies found that unmodified HRAS associates with BRAF but not CRAF.[22] However, BRET assays suggest that CRAF does not show preference for either H- or KRAS, while BRAF appears to prefer KRAS.[33] This preference is suggested to result from the potential favorable interactions between the negatively charged BSR of BRAF and the positively charged, poly-lysine region of the HVR of KRAS.[33] The conflicting studies highlight the complexity of this signaling pathway. Our binding data provide additional examples of isoform-specific activity. We speculate that diminished BRAF-NT1 binding to HRAS and increased BSR exposure upon HRAS binding may be due to electrostatic repulsion between HRAS and the BSR. Our full-length KRAS and its interaction with NT1 support the hypothesis that the BSR attenuates fast binding to HRAS but not to KRAS. Despite the synergistic effect of the BSR, RBD, and CRD in preferring autoinhibitory interactions, the opposite charge attraction between the BSR and KRAS can overcome this preference and speed up the relief of autoinhibition upon binding. Our results provide insight into the complexities of isoform-specific interactions, which are clearly important given that RAS and RAF isoforms display specific levels of activity in mutant and wildtype cells. For example, KRAS is responsible for most RAS-driven cancers[34], and BRAF has the highest basal activity among RAF isoforms.[31]

In recent years, two significant studies resolved the structure of autoinhibited, monomeric BRAF in complex with MEK and 14-3-3.[18,29] These studies revealed that the CRD is cradled within 14-3-3 protomers, which interact with phosphoserines at the N- and C-terminal regions of BRAF. In this conformation, the CRD interacts with the KD, while the membrane-binding loops of the CRD are occluded by 14-3-3.[18] Our results that N-terminal constructs without the CRD do not bind to the KD support the critical role of the CRD. Because the BSR is highly flexible, it was not resolved in either cryo-EM structure. Our constructs including the BSR provide valuable insight into this domain. Comparison of constructs with and without the BSR shows that the BSR, in synchronism with the CRD, increases the affinity of BRAF for the kinase domain, thereby revealing it as a potential target for novel drug design to maintain autoinhibition and prevent activation of BRAF. Our results that NT1 has a higher affinity for KD than NT3 align well with the previous report that the BRAF has higher autoinhibitory activity than CRAF,[32] as NT3 of BRAF is more alike to the N-terminal of CRAF which does not have the BSR. We speculate that the BSR in BRAF exhibits allosteric effect to enforce the autoinhibitory interactions between the CRD and KD. The CRD is a hotspot of RASopathy mutations in BRAF, with the most common mutant, Q257R, activating the MAPK pathway.[45,46] While RASopathy mutations in BRAF are centered within the CRD, our results imply that the mutations may also affect the ability of the BSR to regulate BRAF autoinhibition.

Recent studies have partially revealed the order of RAF activation events through static structures[18,27–29] and live-cell studies with mutant KRAS.[32] Martinez Fiesco *et al.* resolved the RBD in the autoinhibited BRAF-MEK-14-3-3 complex, which revealed that the RBD forms a large interface with one of the 14-3-3 protomers and that RBD-KRAS contact residues are exposed and available to form bonds with RAS.[29] Structural analysis predicts that the RBD-CRD interactions with RAS and the membrane disrupt the autoinhibitory interactions with 14-3-3 and the kinase domain due to overlap in these binding regions.[34] We show, through definitive biochemical methods, that RAS binding directly forces BRAF out of autoinhibition and primes it for subsequent activating steps. Our *in vitro* binding studies are the first of all kind, and align with previous implications that RAS relieves RAF autoinhibition.[41] Additionally, we found that the oncogenic potential of $BRAF^{D594G}$ is propelled through a decreased autoinhibitory potential. Together, these findings suggest that the autoinhibited conformation of wild-type BRAF is not capable of dimerizing, further supporting the model that BRAF binding to HRAS relieves autoinhibition and initiates the activation process. Once autoinhibition is relieved, subsequent dimerization becomes possible, leading to full activation of BRAF. Class 3 BRAF mutants, like $BRAF^{D594G}$, have been shown to bind to active RAS more efficiently than $BRAF^{WT}$.[47] This may be due to the fact that the attenuated autoinhibitory interactions make the RBD and CRD more accessible to RAS. These observations demonstrate the importance of considering mutations from an autoinhibitory standpoint and therapeutically maintaining autoinhibition to treat RAS-dependent BRAF cancers.

We present a comprehensive set of *in vitro* quantitative binding affinities for BRAF-NTs, BRAF-KD, and HRAS, shedding light on the roles of BRAF N-terminal domains in activation and regulation. Our *in vitro* studies were conducted using proteins purified from *E. coli*, which lack the membrane, post-translational modifications, and regulatory, scaffolding, or chaperone proteins that are involved in BRAF regulation. Nonetheless, our study provides a direct characterization of the intra- and inter-molecular protein-protein interactions involved in BRAF regulation, without the complications that arise in cell-based assays. Our findings extend current

knowledge of BRAF regulation and provide novel insight into the development of next-generation BRAF therapy. Our study reveals the previously understudied BSR as a critical modulator of BRAF activation and RAS-binding specificity. Additionally, our experimental setup provides a potential framework for testing inhibitors against RAS-RAF interaction. Allosteric inhibitors stabilizing the autoinhibited conformation of BRAF could be a promising strategy against oncogenic KRAS, especially since it is the primary RAS isoform responsible for activating BRAF.

Experimental methods

Plasmids GST-HRAS and His/MBP-KRAS were purchased from Addgene (#55653 and # 159546). GST-KRAS was created with standard Gibson Assembly (NEB) procedures with pGEX2T as the vector and the following primers: 5'ATCTGGTTCCGCGTGGATCCACTGAA-TATAAACTTGTGGTAG 3' (GST-KRAS_For), 5' CAGTCAGTCAC-GATGAATTCTTACATAATTACACACTTTGTCTTTG 3' (GST-KRAS_Rev), 5' GAATTCATCGTGACTGACTGACG 3' (GST-vector_For), 5' GGATCCACGCGGAACCAG 3' (GST-vector_Rev). 6xHis-KD^{WT} and 6xHis-KD^{D594G} were designed as described previously (amino acids 442-723 with 16 solubilizing mutations: I543A, I544S, I551 K, Q562R, L588N, K630S, F667E, Y673S, A688R, L706S, Q709R, S713E, L716E, S720E, P722S, and K723G).[42] His/MBP-BRAF NTs were created with standard Gibson Assembly (NEB) procedure in the pET28-MBP vector from the following primers: 5' CATATGCTCG-GATCCGCGGCGCTGAGCGGTG 3' (BRAF-RBD_For 1), 5' CATATGCTCGGATCCTCAC-CACAAAAACCTATCGTTAG 3' (BRAF-RBD_For 151), 5' GTTGTAAGAATTCAA-GCTTACAACACTTCCACATGCAATTC 3' (BRAF-RBD_Rev 227), 5' CAAA-GAACTGAATTCAAGCTTACAAATCAAGTTGGT 3' (BRAF-RBD_Rev 288).

Protein expression All protein construct plasmids were transformed into BL21 codon + *E. coli.* and grown to an OD_{600} 0.6-0.8 in LB broth (BRAF NT constructs supplemented with 100 µM $ZnCl_2$), followed by induction with 0.4 mM IPTG. Cells were left overnight at 18 °C, shaking 210 rpm. Cells were pelleted, flash frozen, and stored at -80 °C.

Dimeric HRAS/KRAS purification. GST-tagged full-length HRAS/KRAS pellet was thawed and incubated with lysis buffer (20 mM HEPES pH 7.4, 150 mM NaCl, 1 mM EDTA, 5% Glycerol, 1 mg/mL lysozyme, and protease inhibitor cocktail) for 1h at room temperature. Whole cell lysate was exposed to brief sonication (HRAS) or passed through the French pressure cell press (KRAS) at 1250 psi and centrifuged. Soluble cell lysate was incubated with pre-equilibrated glutathione resin for 1 h at 4°C. After extensive washing, HRAS protein was eluted off the resin with elution buffer (20 mM HEPES pH 7.4, 150 mM NaCl, 1 mM EDTA, 5% Glycerol, and 10 mM reduced glutathione). To dissociate bound nucleotide, HRAS was incubated in HEPES buffer with 10 mM EDTA and 10 M excess GMPPNP (Sigma-Aldrich) for 30 min at 4 °C. To allow rebinding, $MgCl_2$ was added to a final concentration of 1M and rotated for 2 h at 4 °C.[48] HRAS was further purified on a Superdex 200 10/300 GL size exclusion chromatography column (Cytiva). Main steps were checked with sds-PAGE followed by Coomassie staining. After concentration, aliquots were flash frozen and stored at -80°C.

BRAF NT purification. After overexpression and induction, cells were pelleted and resuspended in lysis buffer (20 mM HEPES pH 8, 150 mM NaCl, 5% glycerol, and protease inhibitor cocktail). Whole cell lysate was exposed to brief sonication and centrifuged. Soluble cell lysate

was incubated with pre-equilibrated Ni-NTA resin for 1 h at 4°C. After extensive washing, BRAF-NT protein was eluted off the resin with elution buffer (20 mM HEPES pH 7.4, 150 mM NaCl, 5% glycerol, and increasing imidazole concentrations [90, 200, 400 mM]). BRAF-NT was further purified on a Superdex 200 10/300 GL size exclusion chromatography column (Cytiva). Main steps were checked with sds-PAGE followed by Coomassie staining. After concentration, aliquots were flash frozen and stored at -80°C.

WT BRAF KD Purification His-tagged wild-type BRAF kinase domain (KD) Pellet was lysed in buffer (50 mM HEPES pH 8.0, 150 mM NaCl, 5% glycerol, 10 mg/mL lysozyme, and protease inhibitor cocktail) for 1 h at room temperature. Whole cell lysate was exposed to brief sonication and centrifuged. Soluble cell lysate was incubated with pre-equilibrated cobalt resin for 2 h at 4°C. Resin was washed three times with low salt buffer (50 mM HEPES pH 8, 150 mM NaCl, and 5% glycerol), three times with high salt buffer (50 mM HEPES pH 8, 400 mM NaCl, and 5% glycerol), and three more times with wash buffer (50 mM HEPES pH 7.4, 150 mM NaCl, and 5% glycerol). Protein was eluted off the resin with elution buffers (50 mM HEPES pH 7.4, 150 mM NaCl, 5% glycerol, and varying imidazole concentrations [400mM, 200mM, 90mM]) starting with the lowest imidazole concentration to the highest for a total of 10 elution fractions. WT BRAF KD was further purified on a Superdex 75 10/300 GL size exclusion chromatography column (Cytiva). Main steps were checked with sds-PAGE followed by Coomassie staining. After concentration, aliquots were flash frozen and stored at -80°C.

BRAF-KD-D594G purification.[42] His-tagged BRAF-KD-D594G Pellet was thawed and resuspended in lysis buffer (50 mM phosphate buffer pH 7.0, 250 mM NaCl, 20 mM Imidazole, 10% Glycerol, and EDTA-free protease inhibitor cocktail tablet). Whole cell lysate was exposed to brief sonication and centrifuged. Soluble cell lysate was incubated with pre-equilibrated Ni-NTA resin for 1 h at 4°C. Protein-resin complex was washed 5x 20 mL with chaperone-removal buffer (50 mM HEPES pH 7.4, 5 mM ATP, 50 mM KCl, 20 mM $MgCl_2$, 20 mM Imidazole) and another 5 x 20 mL washes with low salt buffer (50 mM HEPES pH 7.4, 250 mM NaCl, 20 mM Imidazole, 10% glycerol). BRAF was eluted with increasing concentrations of Imidazole (50-400 mM), pooled, and concentrated. Concentrated BRAF was further refined on a Superdex 200 10/300 GL column (Cytiva). Protein was concentrated, aliquoted, flash frozen and stored at -80°C.

Pulldowns. All proteins were added in 1:1 stoichiometric ratio and incubated together in binding buffer (50 mM HEPES pH 7.4, 150 mM NaCl, 5% Glycerol, and 0.125 mg/mL BSA) with 20 µL of glutathione sepharose 4b resin (Cytiva), amylose resin (NEB), or Pierce streptavidin magnetic beads (ThermoScientific). After extensive washing (50 mM HEPES pH 7.4, 500 mM NaCl, 5% Glycerol, and 0.125 mg/mL BSA), 30 µL 4x loading dye was added to resin. Supernatant were loaded and protein analyzed through sds-PAGE. After transfer to nitrocellulose membrane, GST-HRAS/-KRAS was probed with GST antibody (Santa Cruz Biotechnologies SC-138), KRAS with RAS antibody (Cell Signaling 67648S) and BRAF NTs/ BRAF KD with His antibody (Sigma SAB5600227). Finally, western blots were imaged on Cytiva *Typhoon* imager.

Biotinylation 1 mg **"**No-weigh Sulfo NHS biotin" (Thermo Scientific) was resuspended in water and immediately added to BRAF-KD in 50 molar excess. Reaction was performed in Thermo Scientific Slide-A-Lyzer MINI Dialysis Unit. Mixture was left at RT rocking for 30-60 min, then

dialysis unit placed in 500 mL dialysis buffer and left at RT for 2 h with gentle mixing. CPC was biotinylated in excess of sulfo-NHS-biotin in 1:1, 2:1, and 4:1 (CPC:biotin) and left for 60 min rotating at RT before direct use.

Hydrogen-Deuterium Exchange Mass Spectrometry Protein samples (BRAF NT2 (60 uM), NT3 (26 uM), or HRAS (40 uM) protein stock in 20 mM HEPES pH 7.4, 150 mM NaCl, 5% glycerol) were exposed to deuterated buffer (D_2O solution containing 20 mM HEPES pH 7.4, 150 mM NaCl, 5% glycerol) by mixing protein stock with D2O buffer in a 1:5 (v:v) ratio for times ranging from 20 sec to 45 h. Exchange was quenched with 1:1 (v:v quench buffer: deuterated-protein buffer solution) cold quench buffer (100 mM phosphate pH 2.4, 0.5 M TCEP, 3 M guanidium chloride) to pH 2.4. The quenched sample was passed through a homemade immobilized pepsin column for digestion. The resulting peptides were trapped and desalted on a small C8 column (Higgins Analytical TARGA C8 5um 5 X 1.0mm). After desalting (3 min at 0C) peptides were eluted by a gradient (8ul/min, 10% to 40% acetonitrile over 15 min) & passed through an analytical column (Higgens Analytical TARGA C8 5um, 50 x 0.3 mm) and introduced into a THERMO Q-Exactive mass spectrometer by electrospray.[49,50]
Peptides were identified by MS/MS analysis of nondeuterated samples. MS/MS data was analyzed by SEQUEST (Thermo Proteome Discoverer) using a sequence database including BRAF NT2, BRAF NT3, HRAS, pepsin and many potential contaminants and decoy proteins. 110 and 183 peptides (BRAF NT2 and NT3, respectively [not including MBP-tag or linker peptides]) were identified by MS/MS of which 35 and 80 (BRAF NT2 and NT3, respectively) were consistently found with good intensity in HX runs and are used here. Deuterated samples were analyzed using ExMS2.[51]

OpenSPR Binding studies of BRAF-KD-WT/D459G to BRAF-NTs were measured using OpenSPR (Nicoya). BRAF-KD-WT/D594G was immobilized (50 ug/ml; ~6000 RU) on a carboxyl sensor chip (Nicoya) following standard manufacturer protocols of the amine coupling kit (Nicoya). Analyte (BRAF-NT at 5, 15, 44, 133, 400 nM) was flowed over the sensor chip in buffer (20 mM HEPES pH 7.4, 150 mM NaCl, 5% glycerol, 0.005% Tween-20, 1% BSA) at a flow rate of 30 µL/min, allowing time for dissociation (10 min), to obtain real-time binding data. To disrupt the interaction, 400 nM BRAF-NT1 was pre-bound with 400 nM HRAS, by rotating at 4°C for 1 h, subsequently 3x diluted in HEPES buffer and flowed over the sensor in the same flow conditions. Binding kinetics were determined by 1:1 fitting model and experiments plotted against each other using Trace Drawer software. K_D values are reported as mean ± standard deviation.

BRAF-NT: RAS interaction. BRAF-NT1-4 were immobilized to at least 2500 RU on Ni-NTA sensor (Nicoya) following manufacturer protocols in buffer (20 mM HEPES pH 7.4, 150 mM NaCl, 0.05% Tween-20). After immobilization, buffer switched to 20 mM HEPES pH 7.4, 150 mM NaCl, 0.23% glycerol, 0.05% Tween-20 for analyte injections (1% BSA added for KRAS injections to reduce non-specific binding). H-/K-RAS was flowed over at 30 µL/min for 10 min at increasing concentrations (12.3, 37.0, 111, 333, 1000 nM, and 3000 nM [KRAS only]) and the chip was regenerated with 10 mM NaOH at 150 µL/min, allowing 3 min for baseline stabilization after each HRAS injection. For slow flow NT1:HRAS experiments, HRAS was flowed over at 5 µL/min for 30 min. Monomeric KRAS was flowed over at 30 uL/min (20 mM HEPES pH 7.4, 150 mM NaCl, 0.05% Tween-20, 1% w:v BSA) for 10 mins at increasing

concentrations (62.5, 125, 250, 500, 1000, 2000 nM). Binding kinetics were determined by 1:1 fitting model using Trace Drawer software. K_D values are reported as mean ± standard deviation.

Acknowledgements

This work was supported by WW Smith Charitable Fund (ZW), NIH R15GM128099 (ZW), and NIH R01GM138671 (ZW). Thanks to Dr. Leland Mayne at the University of Pennsylvania for technical support and data analysis of HDX-MS.

References

(1) Lavoie, H.; Therrien, M. Regulation of RAF Protein Kinases in ERK Signalling. *Nature Reviews Molecular Cell Biology*. Nature Publishing Group April 23, 2015, pp 281–298. https://doi.org/10.1038/nrm3979.

(2) Malumbres, M.; Barbacid, M. RAS Oncogenes: The First 30 Years. *Nat. Rev. Cancer* **2003**, *3* (6), 459–465. https://doi.org/10.1038/nrc1097.

(3) Zhang, X. F.; Settleman, J.; Kyriakis, J.; Takeuchi-Suzuki, E.; Elledge, S. J.; Marshall, M. S.; Bruder, J. T.; Rapp, U. R.; Avruch, J. Normal and Oncogenic P21ras Proteins Bind to the Amino-Terminal Regulatory Domain of c-Raf-1. *Nature* **1993**, *364* (6435), 308–313. https://doi.org/10.1038/364308a0.

(4) Vojtek, A. B.; Hollenberg, S. M.; Cooper, J. A. Mammalian Ras Interacts Directly with the Serine/Threonine Kinase Raf. *Cell* **1993**, *74* (1), 205–214. https://doi.org/10.1016/0092-8674(93)90307-C.

(5) Cutler, R. E.; Stephens, R. M.; Saracino, M. R.; Morrison, D. K. Autoregulation of the Raf-1 Serine/Threonine Kinase. *Proc. Natl. Acad. Sci. U. S. A.* **1998**, *95* (16), 9214–9219. https://doi.org/10.1073/pnas.95.16.9214.

(6) Tran, N. H.; Frost, J. A. Phosphorylation of Raf-1 by P21-Activated Kinase 1 and Src Regulates Raf-1 Autoinhibition. *J. Biol. Chem.* **2003**, *278* (13), 11221–11226. https://doi.org/10.1074/jbc.M210318200.

(7) Rajakulendran, T.; Sahmi, M.; Lefrançois, M.; Sicheri, F.; Therrien, M. A Dimerization-Dependent Mechanism Drives RAF Catalytic Activation. *Nature* **2009**, *461*, 542–545. https://doi.org/10.1038/nature08314.

(8) Crews, C. M.; Erikson, R. L. Purification of a Murine Protein-Tyrosine/Threonine Kinase That Phosphorylates and Activates the Erk-1 Gene Product: Relationship to the Fission Yeast Byr1 Gene Product. *Proc. Natl. Acad. Sci. U. S. A.* **1992**, *89* (17), 8205–8209. https://doi.org/10.1073/pnas.89.17.8205.

(9) Yoon, S.; Seger, R. The Extracellular Signal-Regulated Kinase: Multiple Substrates Regulate Diverse Cellular Functions. *Growth Factors* **2006**, *24* (1), 21–44. https://doi.org/10.1080/02699050500284218.

(10) Prior, I. A.; Lewis, P. D.; Mattos, C. A Comprehensive Survey of Ras Mutations in Cancer. *Cancer Res.* **2012**, *72* (10), 2457–2467. https://doi.org/10.1158/0008-5472.CAN-11-2612.

(11) Davies, H.; Bignell, G. R.; Cox, C.; Stephens, P.; Edkins, S.; Clegg, S.; Teague, J.; Woffendin, H.; Garnett, M. J.; Bottomley, W.; Davis, N.; Dicks, E.; Ewing, R.; Floyd, Y.; Gray, K.; Hall, S.; Hawes, R.; Hughes, J.; Kosmidou, V.; Menzies, A.; Mould, C.; Parker, A.; Stevens, C.; Watt, S.; Hooper, S.; Jayatilake, H.; Gusterson, B. A.; Cooper, C.; Shipley, J.; Hargrave, D.; Pritchard-Jones, K.; Maitland, N.; Chenevix-Trench, G.; Riggins, G. J.; Bigner, D. D.; Palmieri, G.; Cossu, A.; Flanagan, A.; Nicholson, A.; Ho, J. W. C.; Leung, S. Y.; Yuen, S. T.; Weber, B. L.; Seigler, H. F.; Darrow, T. L.; Paterson, H.; Wooster, R.; Stratton, M. R.; Futreal, P. A. Mutations of the BRAF Gene in Human Cancer. *Nature* **2002**, *417* (6892), 949–954. https://doi.org/10.1038/nature00766.

(12) Tajan, M.; Paccoud, R.; Branka, S.; Edouard, T.; Yart, A. The RASopathy Family: Consequences of Germline Activation of the RAS/MAPK Pathway. *Endocrine Reviews*. Oxford University Press October 1, 2018, pp 676–700. https://doi.org/10.1210/er.2017-00232.

(13) Canon, J.; Rex, K.; Saiki, A. Y.; Mohr, C.; Cooke, K.; Bagal, D.; Gaida, K.; Holt, T.; Knutson, C. G.; Koppada, N.; Lanman, B. A.; Werner, J.; Rapaport, A. S.; San Miguel, T.; Ortiz, R.; Osgood, T.; Sun, J. R.; Zhu, X.; McCarter, J. D.; Volak, L. P.; Houk, B. E.; Fakih, M. G.; O'Neil, B. H.; Price, T. J.; Falchook, G. S.; Desai, J.; Kuo, J.; Govindan, R.; Hong, D. S.; Ouyang, W.; Henary, H.; Arvedson, T.; Cee, V. J.; Lipford, J. R. The Clinical KRAS(G12C) Inhibitor AMG 510 Drives Anti-Tumour Immunity. *Nat. 2019 5757781* **2019**, *575* (7781), 217–223. https://doi.org/10.1038/s41586-019-1694-1.

(14) Fell, J. B.; Fischer, J. P.; Baer, B. R.; Blake, J. F.; Bouhana, K.; Briere, D. M.; Brown, K. D.; Burgess, L. E.; Burns, A. C.; Burkard, M. R.; Chiang, H.; Chicarelli, M. J.; Cook, A. W.; Gaudino, J. J.; Hallin, J.; Hanson, L.; Hartley, D. P.; Hicken, E. J.; Hingorani, G. P.; Hinklin, R. J.; Mejia, M. J.; Olson, P.; Otten, J. N.; Rhodes, S. P.; Rodriguez, M. E.; Savechenkov, P.; Smith, D. J.; Sudhakar, N.; Sullivan, F. X.; Tang, T. P.; Vigers, G. P.; Wollenberg, L.; Christensen, J. G.; Marx, M. A. Identification of the Clinical Development Candidate MRTX849, a Covalent KRASG12C Inhibitor for the Treatment of Cancer. *J. Med. Chem.* **2020**, *63* (13), 6679–6693. https://doi.org/10.1021/ACS.JMEDCHEM.9B02052.

(15) Yao, Z.; Torres, N. M.; Tao, A.; Gao, Y.; Luo, L.; Li, Q.; de Stanchina, E.; Abdel-Wahab, O.; Solit, D. B.; Poulikakos, P. I.; Rosen, N. BRAF Mutants Evade ERK-Dependent Feedback by Different Mechanisms That Determine Their Sensitivity to Pharmacologic Inhibition. *Cancer Cell* **2015**, *28* (3), 370–383. https://doi.org/10.1016/J.CCELL.2015.08.001.

(16) Hatzivassiliou, G.; Song, K.; Yen, I.; Brandhuber, B. J.; Anderson, D. J.; Alvarado, R.; Ludlam, M. J. C.; Stokoe, D.; Gloor, S. L.; Vigers, G.; Morales, T.; Aliagas, I.; Liu, B.; Sideris, S.; Hoeflich, K. P.; Jaiswal, B. S.; Seshagiri, S.; Koeppen, H.; Belvin, M.; Friedman, L. S.; Malek, S. RAF Inhibitors Prime Wild-Type RAF to Activate the MAPK Pathway and Enhance Growth. *Nature* **2010**, *464* (7287), 431–435. https://doi.org/10.1038/nature08833.

(17) Poulikakos, P. I.; Zhang, C.; Bollag, G.; Shokat, K. M.; Rosen, N. RAF Inhibitors Transactivate RAF Dimers and ERK Signalling in Cells with Wild-Type BRAF. *Nature* **2010**, *464* (7287), 427–430. https://doi.org/10.1038/nature08902.

(18) Park, E.; Rawson, S.; Li, K.; Kim, B. W.; Ficarro, S. B.; Pino, G. G. Del; Sharif, H.; Marto, J. A.; Jeon, H.; Eck, M. J. Architecture of Autoinhibited and Active BRAF–MEK1–14-3-3 Complexes. *Nature* **2019**, *575* (7783), 545–550. https://doi.org/10.1038/s41586-019-1660-y.

(19) Kyriakis, J. M.; App, H.; Zhang, X. F.; Banerjee, P.; Brautigan, D. L.; Rapp, U. R.; Avruch, J. Raf-1 Activates MAP Kinase-Kinase. *Nature* **1992**, *358* (6385), 417–421. https://doi.org/10.1038/358417a0.

(20) Roy, S.; Lane, A.; Yan, J.; McPherson, R.; Hancock, J. F. Activity of Plasma Membrane-Recruited Raf-1 Is Regulated by Ras via the Raf Zinc Finger. *J. Biol. Chem.* **1997**, *272* (32), 20139–20145. https://doi.org/10.1074/jbc.272.32.20139.

(21) Ghosh, S.; Xie, W. Q.; Quest, A. F. G.; Mabrouk, G. M.; Strum, J. C.; Bell, R. M. The Cysteine-Rich Region of Raf-1 Kinase Contains Zinc, Translocates to Liposomes, and Is Adjacent to a Segment That Binds GTP-Ras. *J. Biol. Chem.* **1994**, *269* (13), 10000–10007. https://doi.org/10.1016/s0021-9258(17)36981-8.

(22) Fischer, A.; Hekman, M.; Kuhlmann, J.; Rubio, I.; Wiese, S.; Rapp, U. R. B- and C-RAF Display Essential Differences in Their Binding to Ras: The Isotype-Specific N Terminus of B-RAF Facilitates Ras Binding. *J. Biol. Chem.* **2007**, *282* (36), 26503–26516. https://doi.org/10.1074/jbc.M607458200.

(23) Li, S.; Jang, H.; Zhang, J.; Nussinov, R. Raf-1 Cysteine-Rich Domain Increases the Affinity of K-Ras/Raf at the Membrane, Promoting MAPK Signaling. *Structure* **2018**, *26* (3), 513-525.e2. https://doi.org/https://doi.org/10.1016/j.str.2018.01.011.

(24) Brtva, T. R.; Drugan, J. K.; Ghosh, S.; Terrell, R. S.; Campbell-Burk, S.; Bell, R. M.; Der, C. J. Two Distinct Raf Domains Mediate Interaction with Ras. *J. Biol. Chem.* **1995**, *270* (17), 9809–9812. https://doi.org/10.1074/jbc.270.17.9809.

(25) Hu, C. D.; Kariya, K. I.; Tamada, M.; Akasaka, K.; Shirouzu, M.; Yokoyama, S.; Kataoka, T. Cysteine-Rich Region of Raf-1 Interacts with Activator Domain of Post-Translationally Modified Ha-Ras. *J. Biol. Chem.* **1995**, *270* (51), 30274–30277. https://doi.org/10.1074/jbc.270.51.30274.

(26) Williams, J. G.; Drugan, J. K.; Yi, G. S.; Clark, G. J.; Der, C. J.; Campbell, S. L. Elucidation of Binding Determinants and Functional Consequences of Ras/Raf-Cysteine-Rich Domain Interactions. *J. Biol. Chem.* **2000**, *275* (29), 22172–22179. https://doi.org/10.1074/jbc.M000397200.

(27) Tran, T. H.; Chan, A. H.; Young, L. C.; Bindu, L.; Neale, C.; Messing, S.; Dharmaiah, S.; Taylor, T.; Denson, J. P.; Esposito, D.; Nissley, D. V.; Stephen, A. G.; McCormick, F.; Simanshu, D. K. KRAS Interaction with RAF1 RAS-Binding Domain and Cysteine-Rich Domain Provides Insights into RAS-Mediated RAF Activation. *Nat. Commun.* **2021**, *12* (1176), 1–16. https://doi.org/10.1038/s41467-021-21422-x.

(28) Cookis, T.; Mattos, C. Crystal Structure Reveals the Full Ras–Raf Interface and Advances Mechanistic Understanding of Raf Activation. *Biomolecules* **2021**, *11* (7), 996. https://doi.org/10.3390/biom11070996.

(29) Martinez Fiesco, J. A.; Durrant, D. E.; Morrison, D. K.; Zhang, P. Structural Insights into the BRAF Monomer-to-Dimer Transition Mediated by RAS Binding. *Nat. Commun.* **2022**, *13* (1). https://doi.org/10.1038/s41467-022-28084-3.

(30) Marais, R.; Light, Y.; Paterson, H. F.; Mason, C. S.; Marshall, C. J. Differential Regulation of Raf-1, A-Raf, and B-Raf by Oncogenic Ras and Tyrosine Kinases *. *J. Biol. Chem.* **1997**, *272* (7), 4378–4383. https://doi.org/10.1074/JBC.272.7.4378.

(31) Emuss, V.; Garnett, M.; Mason, C.; Marais, R. Mutations of C-RAF Are Rare in Human Cancer Because C-RAF Has a Low Basal Kinase Activity Compared with B-RAF. *Cancer Res.* **2005**, *65* (21), 9719–9726. https://doi.org/10.1158/0008-5472.CAN-05-1683.

(32) Spencer-Smith, R.; Terrell, E. M.; Insinna, C.; Agamasu, C.; Wagner, M. E.; Ritt, D. A.; Stauffer, J.; Stephen, A. G.; Morrison, D. K. RASopathy Mutations Provide Functional Insight into the BRAF Cysteine-Rich Domain and Reveal the Importance of Autoinhibition in BRAF Regulation. *Mol. Cell* **2022**, *82* (22), 4262-4276.e5. https://doi.org/10.1016/J.MOLCEL.2022.10.016.

(33) Terrell, E. M.; Durrant, D. E.; Ritt, D. A.; Sealover, N. E.; Sheffels, E.; Spencer-Smith, R.; Esposito, D.; Zhou, Y.; Hancock, J. F.; Kortum, R. L.; Morrison, D. K. Distinct Binding Preferences between Ras and Raf Family Members and the Impact on Oncogenic Ras Signaling. *Mol. Cell* **2019**, *76* (6), 872-884.e5. https://doi.org/10.1016/j.molcel.2019.09.004.

(34) Simanshu, D. K.; Morrison, D. K. A Structure Is Worth a Thousand Words: New Insights for RAS and RAF Regulation. *Cancer Discov.* **2022**, *12* (4), 899–912. https://doi.org/10.1158/2159-8290.CD-21-1494.

(35) Jumper, J.; Evans, R.; Pritzel, A.; Green, T.; Figurnov, M.; Ronneberger, O.; Tunyasuvunakool, K.; Bates, R.; Žídek, A.; Potapenko, A.; Bridgland, A.; Meyer, C.; Kohl, S. A. A.; Ballard, A. J.; Cowie, A.; Romera-Paredes, B.; Nikolov, S.; Jain, R.; Adler, J.; Back, T.; Petersen, S.; Reiman, D.; Clancy, E.; Zielinski, M.; Steinegger, M.; Pacholska, M.; Berghammer, T.; Bodenstein, S.; Silver, D.; Vinyals, O.; Senior, A. W.; Kavukcuoglu, K.; Kohli, P.; Hassabis, D.; Hassabis, D. Highly Accurate Protein Structure Prediction with AlphaFold. *Nature* **2021**, *596*, 583. https://doi.org/10.1038/s41586-021-03819-2.

(36) Varadi, M.; Anyango, S.; Deshpande, M.; Nair, S.; Natassia, C.; Yordanova, G.; Yuan, D.; Stroe, O.; Wood, G.; Laydon, A.; Zídek, A.; Green, T.; Tunyasuvunakool, K.; Petersen, S.; Jumper, J.; Clancy, E.; Green, R.; Vora, A.; Lutfi, M.; Figurnov, M.; Cowie, A.; Hobbs, N.; Kohli, P.; Kleywegt, G.; Birney, E.; Hassabis, D.; Velankar, S. AlphaFold Protein Structure Database: Massively Expanding the Structural Coverage of Protein-Sequence Space with High-Accuracy Models. *Nucleic Acids Res.* **2022**, *50* (D1), D439–D444. https://doi.org/10.1093/NAR/GKAB1061.

(37) Fetics, S. K.; Guterres, H.; Kearney, B. M.; Buhrman, G.; Ma, B.; Nussinov, R.; Mattos, C. Allosteric Effects of the Oncogenic Rasq61l Mutant on Raf-RBD. *Structure* **2015**, *23* (3), 505–516. https://doi.org/10.1016/j.str.2014.12.017.

(38) Fabian, J. R.; Vojtek, A. B.; Cooper, J. A.; Morrison, D. K. A Single Amino Acid Change

in Raf-1 Inhibits Ras Binding and Alters Raf-1 Function. *Proc. Natl. Acad. Sci. U. S. A.* **1994**, *91* (13), 5982–5986. https://doi.org/10.1073/pnas.91.13.5982.

(39) Prior, I. A.; Hancock, J. F. Ras Trafficking, Localization and Compartmentalized Signalling. *Semin. Cell Dev. Biol.* **2012**, *23* (2), 145–153.

(40) Winkler, D. G.; Cutler, R. E.; Drugan, J. K.; Campbell, S.; Morrison, D. K.; Cooper, J. A. Identification of Residues in the Cysteine-Rich Domain of Raf-1 That Control Ras Binding and Raf-1 Activity. *J. Biol. Chem.* **1998**, *273* (34), 21578–21584. https://doi.org/10.1074/jbc.273.34.21578.

(41) Tran, N. H.; Wu, X.; Frost, J. A. B-Raf and Raf-1 Are Regulated by Distinct Autoregulatory Mechanisms. *J. Biol. Chem.* **2005**, *280* (16), 16244–16253. https://doi.org/10.1074/jbc.M501185200.

(42) Cope, N. J.; Novak, B.; Liu, Z.; Cavallo, M.; Gunderwala, A. Y.; Connolly, M.; Wang, Z. Analyses of the Oncogenic BRAF ^{D594G} Variant Reveal a Kinase-Independent Function of BRAF in Activating MAPK Signaling. *J. Biol. Chem.* **2020**, jbc.RA119.011536. https://doi.org/10.1074/jbc.RA119.011536.

(43) Nieto, P.; Ambrogio, C.; Esteban-Burgos, L.; Gómez-López, G.; Blasco, M. T.; Yao, Z.; Marais, R.; Rosen, N.; Chiarle, R.; Pisano, D. G.; Barbacid, M.; Santamaría, D. A Braf Kinase-Inactive Mutant Induces Lung Adenocarcinoma. *Nature* **2017**, *548* (7666), 239–243. https://doi.org/10.1038/nature23297.

(44) Yan, J.; Roy, S.; Apolloni, A.; Lane, A.; Hancock, J. F. Ras Isoforms Vary in Their Ability to Activate Raf-1 and Phosphoinositide 3-Kinase. *J. Biol. Chem.* **1998**, *273* (37), 24052–24056. https://doi.org/10.1074/JBC.273.37.24052.

(45) Niihori, T.; Aoki, Y.; Narumi, Y.; Neri, G.; Cavé, H.; Verloes, A.; Okamoto, N.; Hennekam, R. C. M.; Gillessen-Kaesbach, G.; Wieczorek, D.; Kavamura, M. I.; Kurosawa, K.; Ohashi, H.; Wilson, L.; Heron, D.; Bonneau, D.; Corona, G.; Kaname, T.; Naritomi, K.; Baumann, C.; Matsumoto, N.; Kato, K.; Kure, S.; Matsubara, Y. Germline KRAS and BRAF Mutations in Cardio-Facio-Cutaneous Syndrome. *Nat. Genet.* **2006**, *38* (3), 294–296. https://doi.org/10.1038/ng1749.

(46) Rodriguez-Viciana, P.; Tetsu, O.; Tidyman, W. E.; Estep, A. L.; Conger, B. A.; Cruz, M. S.; McCormick, F.; Rauen, K. A. Germline Mutations in Genes within the MAPK Pathway Cause Cardio-Facio-Cutaneous Syndrome. *Science (80-.).* **2006**, *311* (5765), 1287–1290. https://doi.org/10.1126/SCIENCE.1124642/SUPPL_FILE/RODRIGUEZ-V.SOM.PDF.

(47) Yao, Z.; Yaeger, R.; Rodrik-Outmezguine, V. S.; Tao, A.; Torres, N. M.; Chang, M. T.; Drosten, M.; Zhao, H.; Cecchi, F.; Hembrough, T.; Michels, J.; Baumert, H.; Miles, L.; Campbell, N. M.; De Stanchina, E.; Solit, D. B.; Barbacid, M.; Taylor, B. S.; Rosen, N. Tumours with Class 3 BRAF Mutants Are Sensitive to the Inhibition of Activated RAS. *Nature* **2017**, *548* (7666), 234–238. https://doi.org/10.1038/nature23291.

(48) Amendola, C. R.; Mahaffey, J. P.; Parker, S. J.; Ahearn, I. M.; Chen, W. C.; Zhou, M.; Court, H.; Shi, J.; Mendoza, S. L.; Morten, M. J.; Rothenberg, E.; Gottlieb, E.; Wadghiri, Y. Z.; Possemato, R.; Hubbard, S. R.; Balmain, A.; Kimmelman, A. C.; Philips, M. R.

KRAS4A Directly Regulates Hexokinase 1. *Nature* **2019**. https://doi.org/10.1038/s41586-019-1832-9.

(49) Mayne, L.; Kan, Z. Y.; Sevugan Chetty, P.; Ricciuti, A.; Walters, B. T.; Englander, S. W. Many Overlapping Peptides for Protein Hydrogen Exchange Experiments by the Fragment Separation-Mass Spectrometry Method. *J. Am. Soc. Mass Spectrom.* **2011**, *22* (11), 1898–1905. https://doi.org/10.1007/S13361-011-0235-4.

(50) Mayne, L. Hydrogen Exchange Mass Spectrometry. *Methods Enzymol.* **2016**, *566*, 356. https://doi.org/10.1016/BS.MIE.2015.06.035.

(51) Z. Y. Kan, X. Ye, J. J. Skinner, L. Mayne, S. W. Englander. ExMS2: An Integrated Solution for Hydrogen-Deuterium Exchange Mass Spectrometry Data Analysis. *Anal Chem* **2019**, *91* (11), 7474–7481.

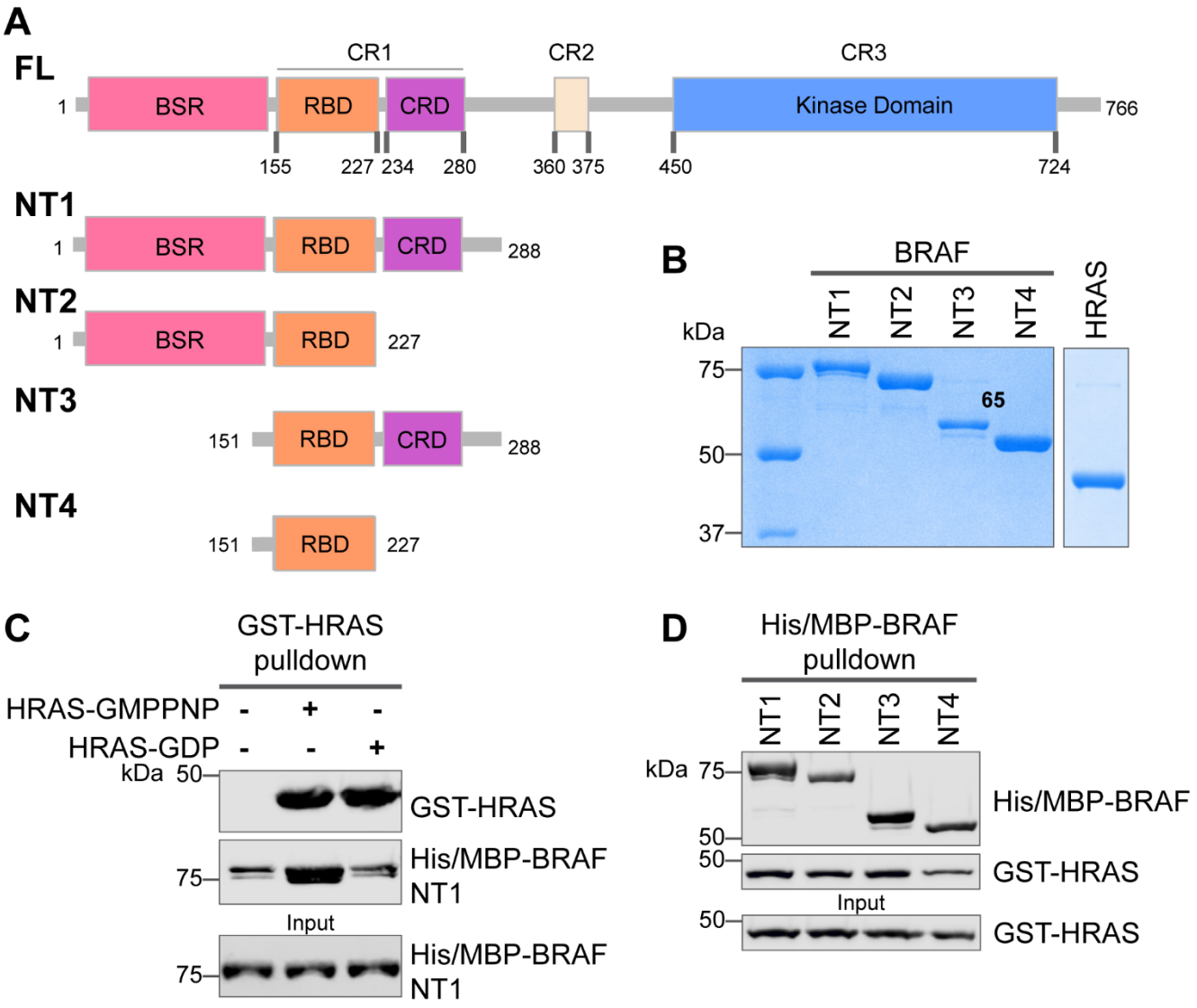

Figure 1. Specific purified N-terminal domains are involved in interacting with HRAS. (A) Diagram of BRAF-NT constructs. Top panel is full-length BRAF, followed by proteins NT1-4 expressed in *E. coli* and purified. Not shown: 6xHis/MBP tag on the N-terminal of NT proteins. BSR= BRAF specific region; RBD=RAS binding domain; CRD= cysteine rich domain. (B) Coomassie stained gels of purified NT1-4 and GST-HRAS. (C) Western blot of HRAS-GMPPNP or HRAS-GDP pulled down on glutathione resin to probe for NT1 binding. (D) Western blot of BRAF NT1-4 pulled down on amylose resin to probe for to HRAS-GMPPNP binding.

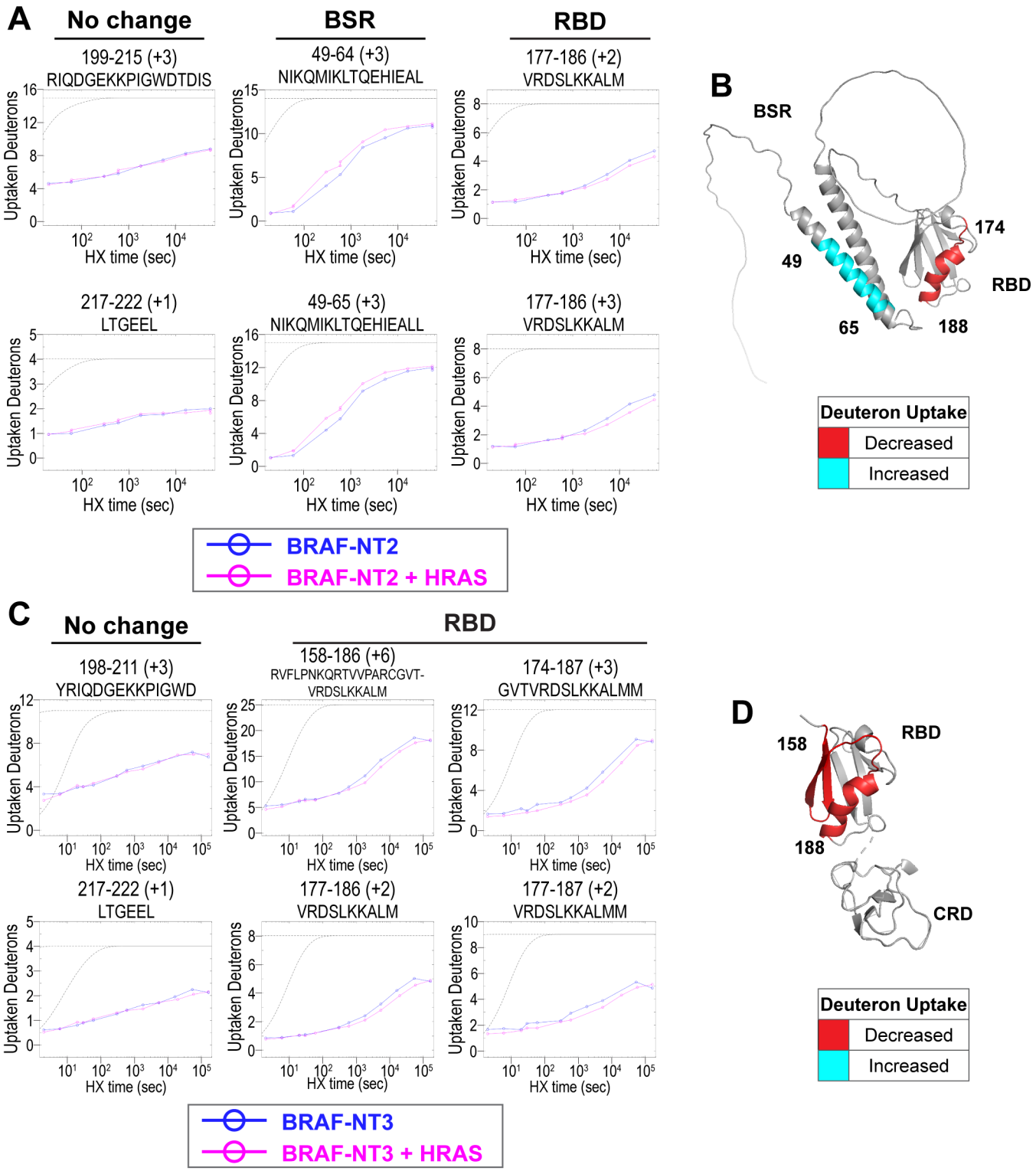

Figure 2. HDX-MS revealed conformational changes of BRAF N-terminal domains in response to HRAS binding. (A, C) Representative NT2 (A) and NT3 (C) peptides identified from HDX-MS in the absence (blue) and presence (pink) of HRAS. Peptides with no change in uptaken

deuterons outside of the binding regions are consistent in both NT2 and NT3. Presented peptide plots displaying differences in uptaken deuterons are representative of a trend of multiple overlapping peptides in the BSR or RBD. (B, D) Deuteron uptake differences of NT2 (B) and NT3 (D) mapped on the predicted BRAF AlphaFold structure, where deuterium is decreased (red) or increased (cyan).

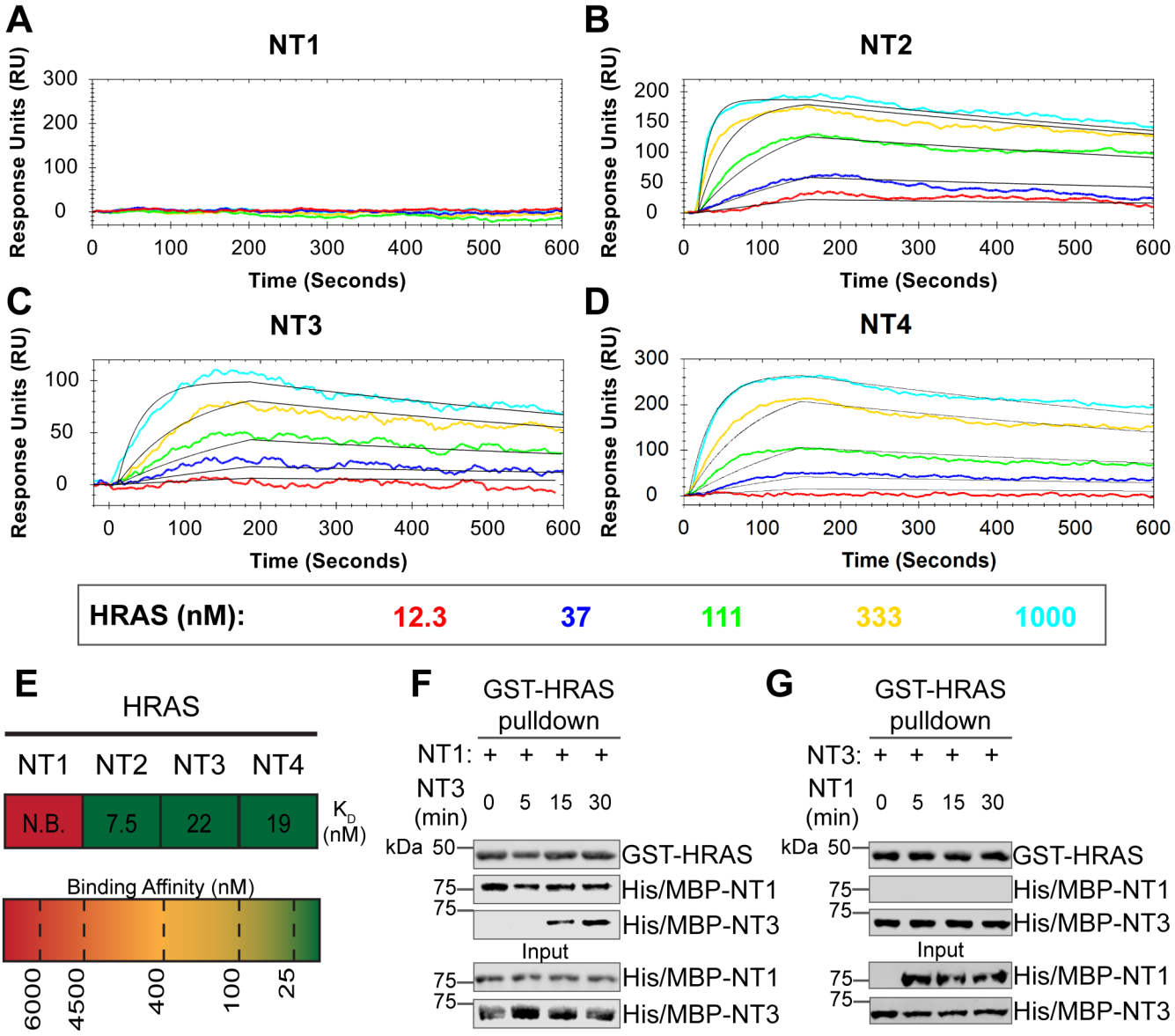

Figure 3. BRAF specific region (BSR) in conjunction with the cysteine rich domain (CRD) reduces binding affinity for HRAS. (A-D) SPR binding curves of HRAS flowed over NT1-4 immobilized on NTA sensors and the best fit curves produced from a 1:1 fitting model kinetic evaluation. Representative of independent experiments with similar results each (NT1: *n=7*, NT2: *n=2*, NT3: *n=2*, NT4: *n=3*). (E) Diagram of the average dissociation constant (K_D) from independent SPR experiments of HRAS flowed over immobilized NT1-4. (F-G) Western blot of purified His/MBP-NT1 (F) or -NT3 (G) binding to GST-HRAS on glutathione resin in a pulldown assay and subsequent competition with NT3 (F) or NT1 (G). Representative of 2 independent experiments each with similar results.

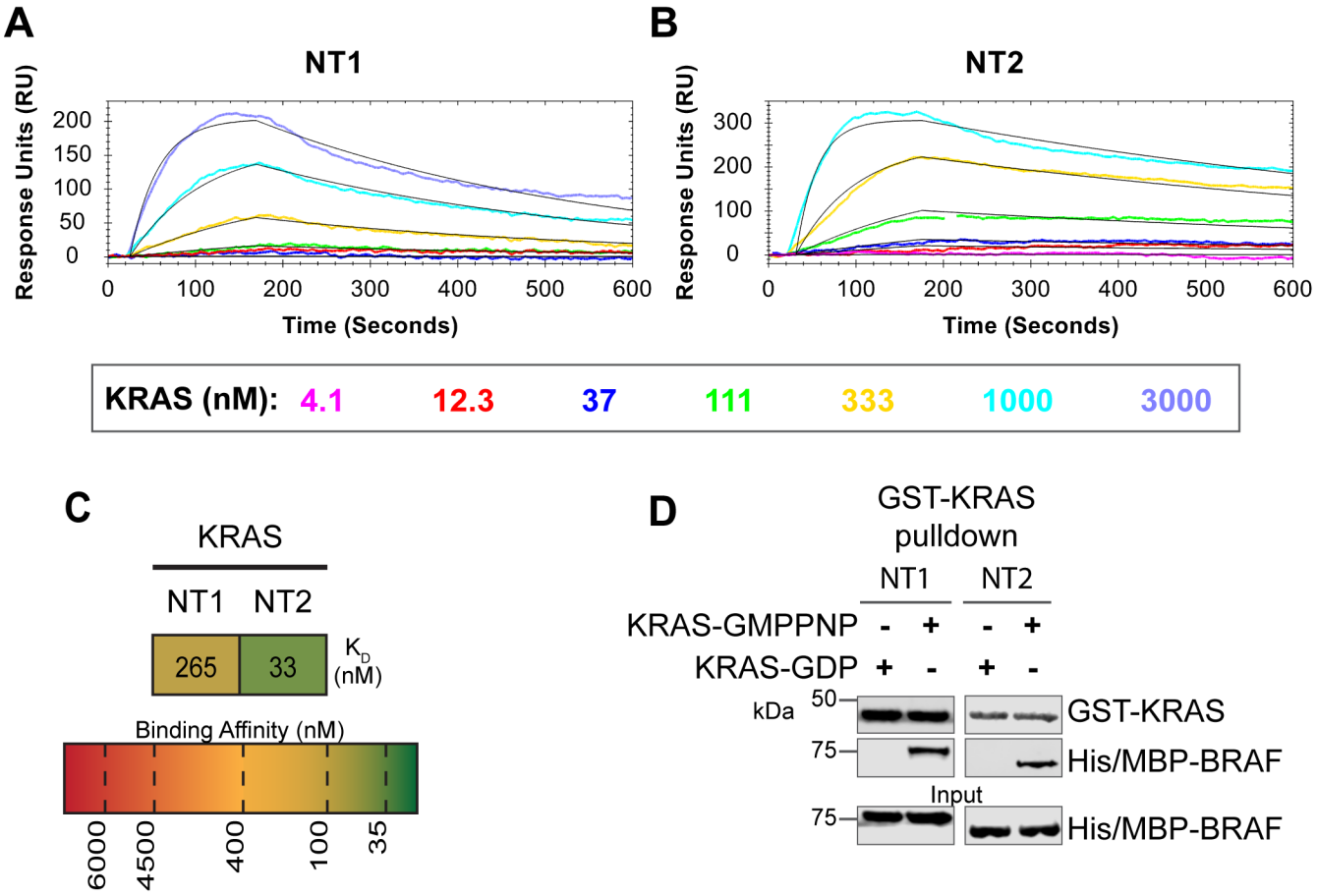

Figure 4. BSR differentiates the BRAF-KRAS interaction from the BRAF-HRAS interaction. (A-B) SPR binding curves of KRAS flowed over NT1 or NT2 immobilized on NTA sensors and the best fit curves produced from a 1:1 fitting model kinetic evaluation. Representative of 2 independent experiments with similar results each. (C) Diagram of the average dissociation constant (K_D) from independent SPR experiments of KRAS flowed over immobilized NT1/NT2. (D) Western blot of purified His/MBP-NT1/2 binding to GST-KRAS on glutathione resin in a pulldown assay. Representative of 2 independent experiments with similar results.

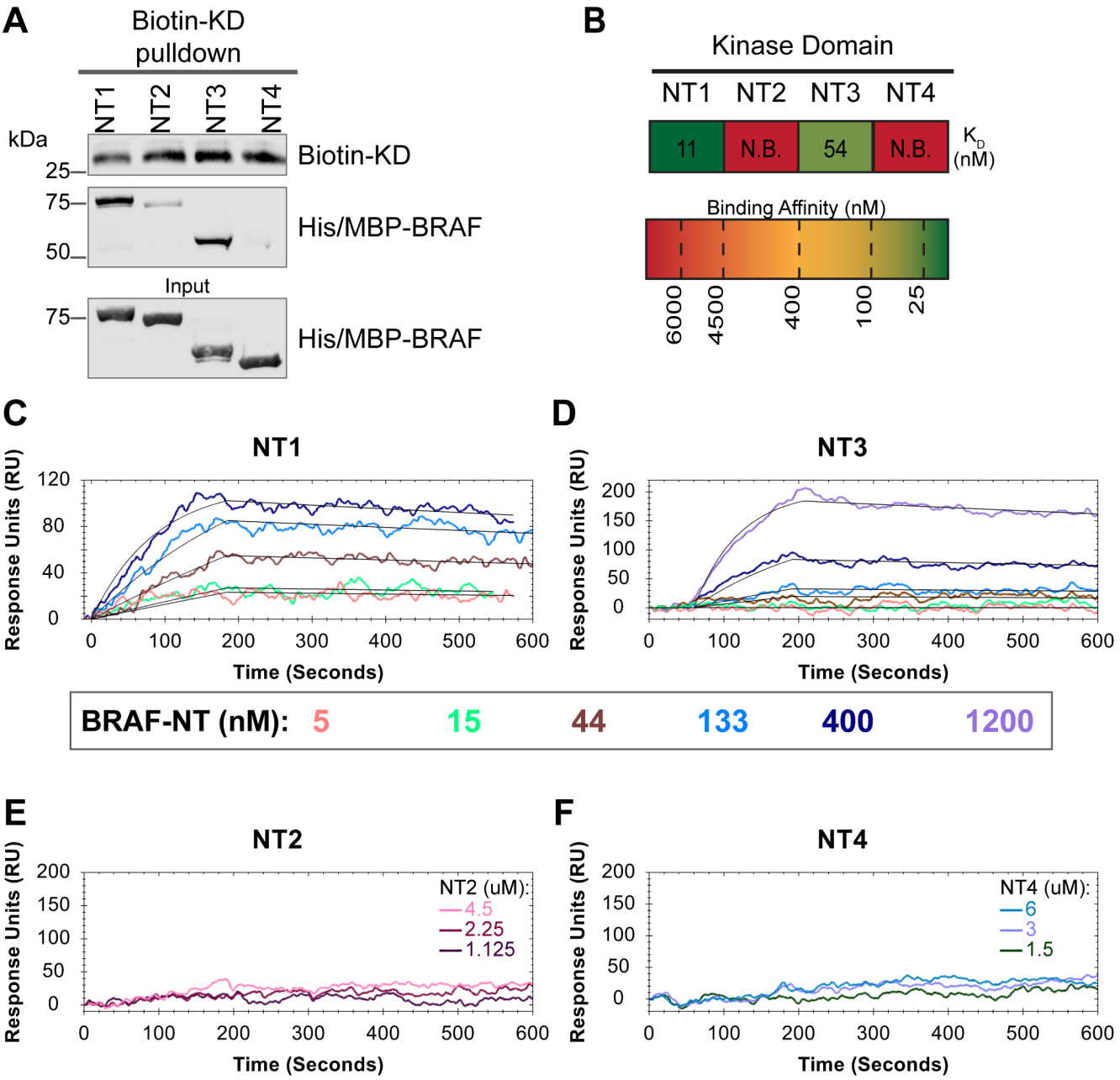

Figure 5. BSR and CRD promote BRAF autoinhibitory interactions. (A) Western blot of purified His/MBP-NT1-4 binding to biotinylated His-KD on streptavidin beads in a pulldown assay. Representative of 3 independent experiments with similar results. (B) Diagram of the average dissociation constant (K_D) from independent SPR experiments of NTs flowed over immobilized KD. (C-D) SPR binding curves of NT1 and NT3 at 5, 15, 44, 133, 400, and 1200 nM (NT3 only) flowed over KD and the best fit curves produced from a 1:1 fitting model kinetic evaluation. Representative of independent experiments with similar results (NT3: *n=2*, NT1: *n=3*). (E-F) No binding of NT2 or NT4 to immobilized KD was observed by SPR even at high

concentrations (NT2: 1.125, 2.25, 4.5 uM; NT4: 1.5, 3, 6 uM). Representative of 2 independent experiments each with similar results.

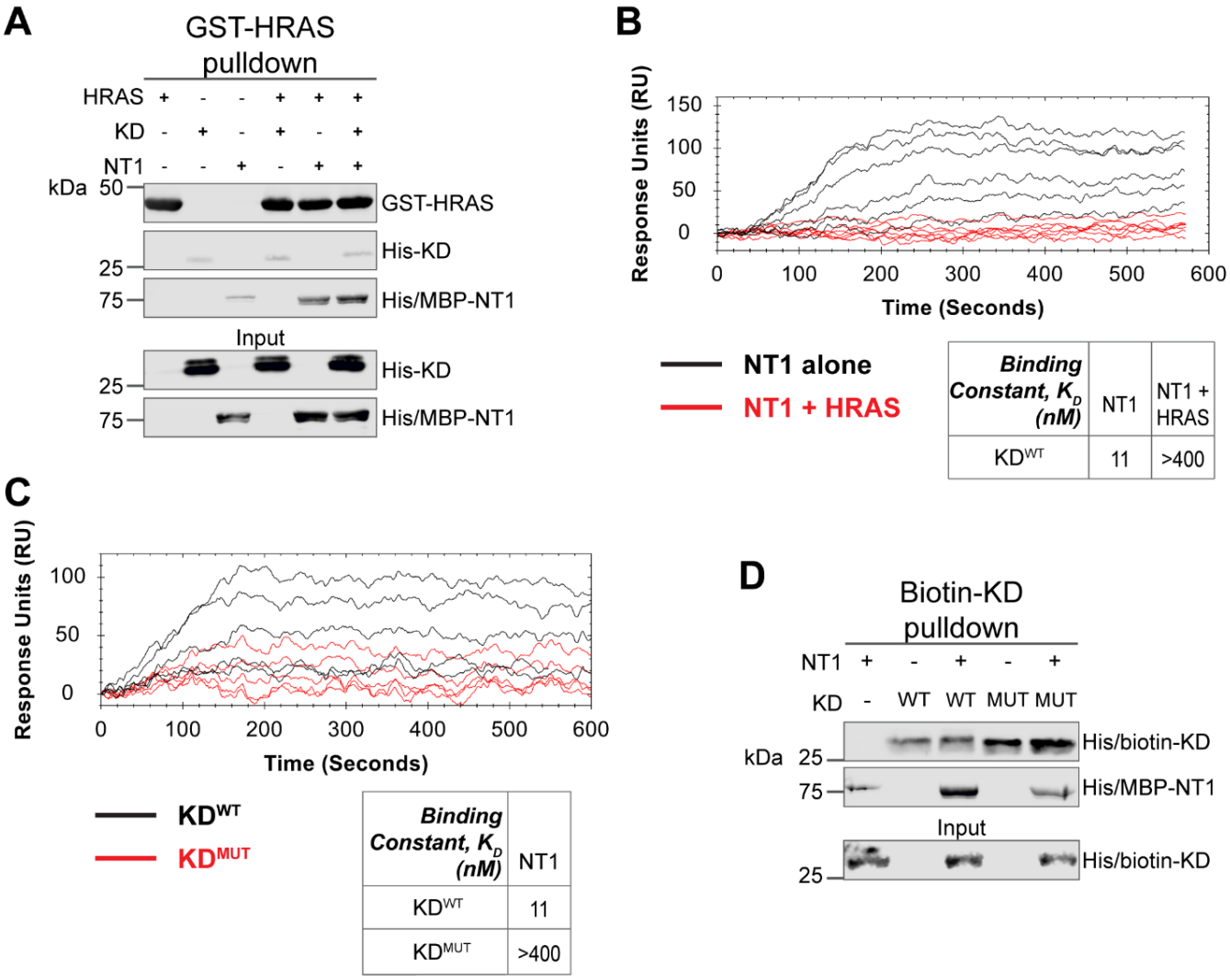

Figure 6. HRAS and KD^{D594G} disrupt BRAF autoinhibition. (A) Western blot of pulldown assay of pre-incubated His/MBP-NT1 and His-KD added to purified GST-HRAS on glutathione resin. Representative data of 2 independent replicates with similar results. (B) SPR experiments in which NT1 at 5, 15, 44, 133, 400 nM (black) and NT1 + HRAS (1:1) at 5, 15, 44, 133, and 400 nM (red) flowed over KD immobilized on carboxyl sensors. Representative data of 3 independent replicates with similar results. (C) SPR experiments of NT1 at 5, 15, 44, 133, and 400 nM flowed over immobilized KD^{WT}(black) or KD^{MUT} (D594G; red) on carboxyl sensors. Representative data of 3 independent replicates with similar results. (D) Western blot of purified His/MBP-NT1 binding to either biotinylated His-KD^{WT} or His-KD^{MUT} (D594G) in pulldown assays on streptavidin beads. Representative data of 3 independent replicates with similar results.

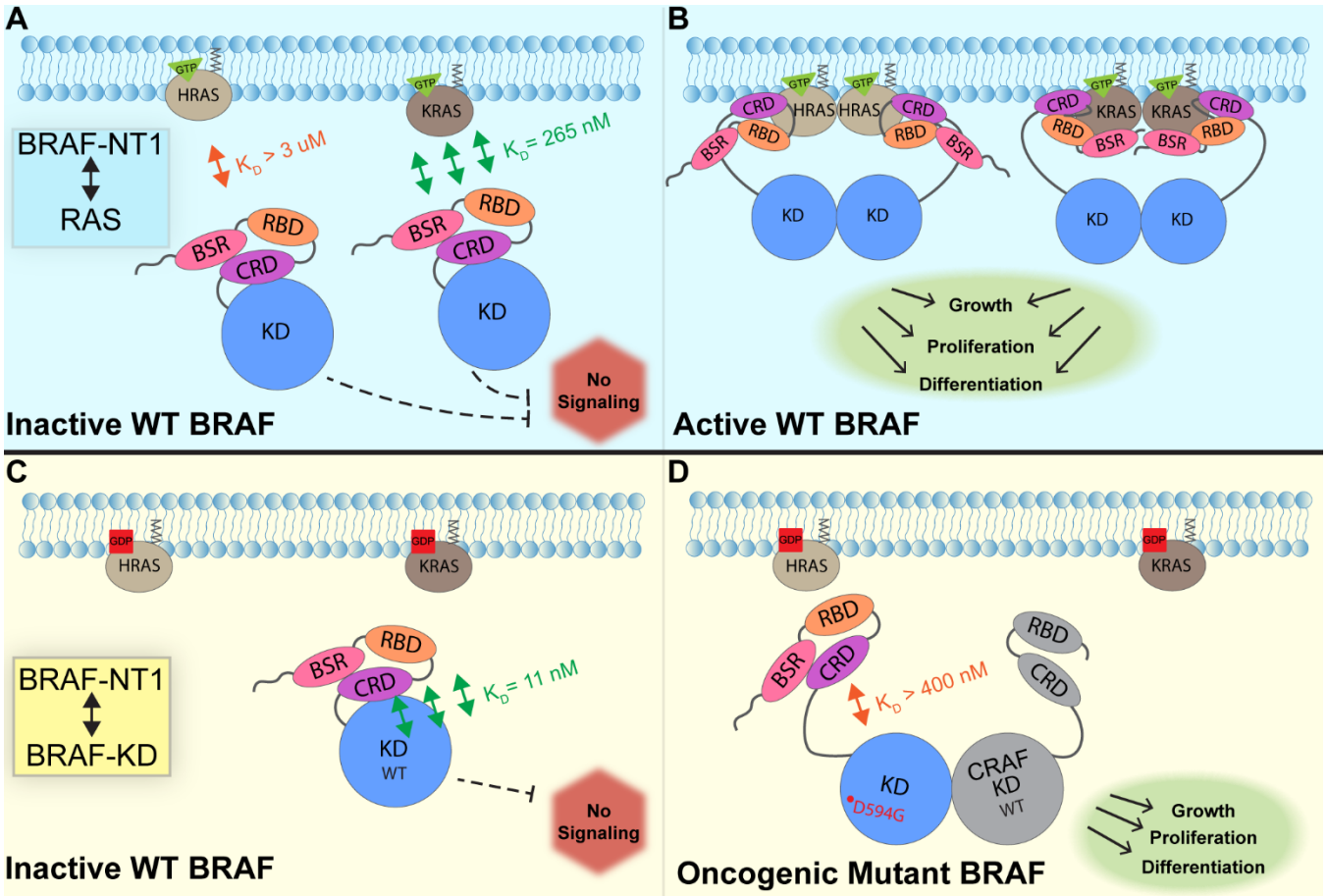

Figure 7. Model of BRAF activation. (A) BRAF is initially an autoinhibited monomer in the cytosol, in which signaling through the RAF-MEK-ERK cascade is not promoted. The BRAF N-terminal region (NT1; aa 1-288), including the BRAF Specific Region (BSR), Cysteine Rich Domain (CRD), and RAS Binding Domain (RBD), interacts with active GTP-bound RAS at the membrane in an isoform specific manner. The BSR increases the affinity of BRAF for KRAS, while decreasing affinity with HRAS, as shown through the different dissociation constants (K_D) determined through OpenSPR. (B) Once bound to active H- or K-RAS, BRAF is unable to remain in the autoinhibited conformation and is subsequently activated upon dimerization, which stimulates signaling for events such as cell growth, proliferation, and differentiation. (C) Tight binding is observed with the BRAF Kinase Domain (KD; aa 442-723) and BRAF NT1, revealing the concerted action of the BSR, RBD, and CRD domains reinforce the autoinhibited conformation and restrict signaling without upstream activation. (D) Oncogenic $BRAF^{D594G}$ stimulates activation of MAPK pathway through a decreased ability to remain in the autoinhibited conformation and an increased potential to dimerize with CRAF. Evading upstream regulation leads to overactivation of the signaling cascade and tumorigenesis.

Supplementary Figures:

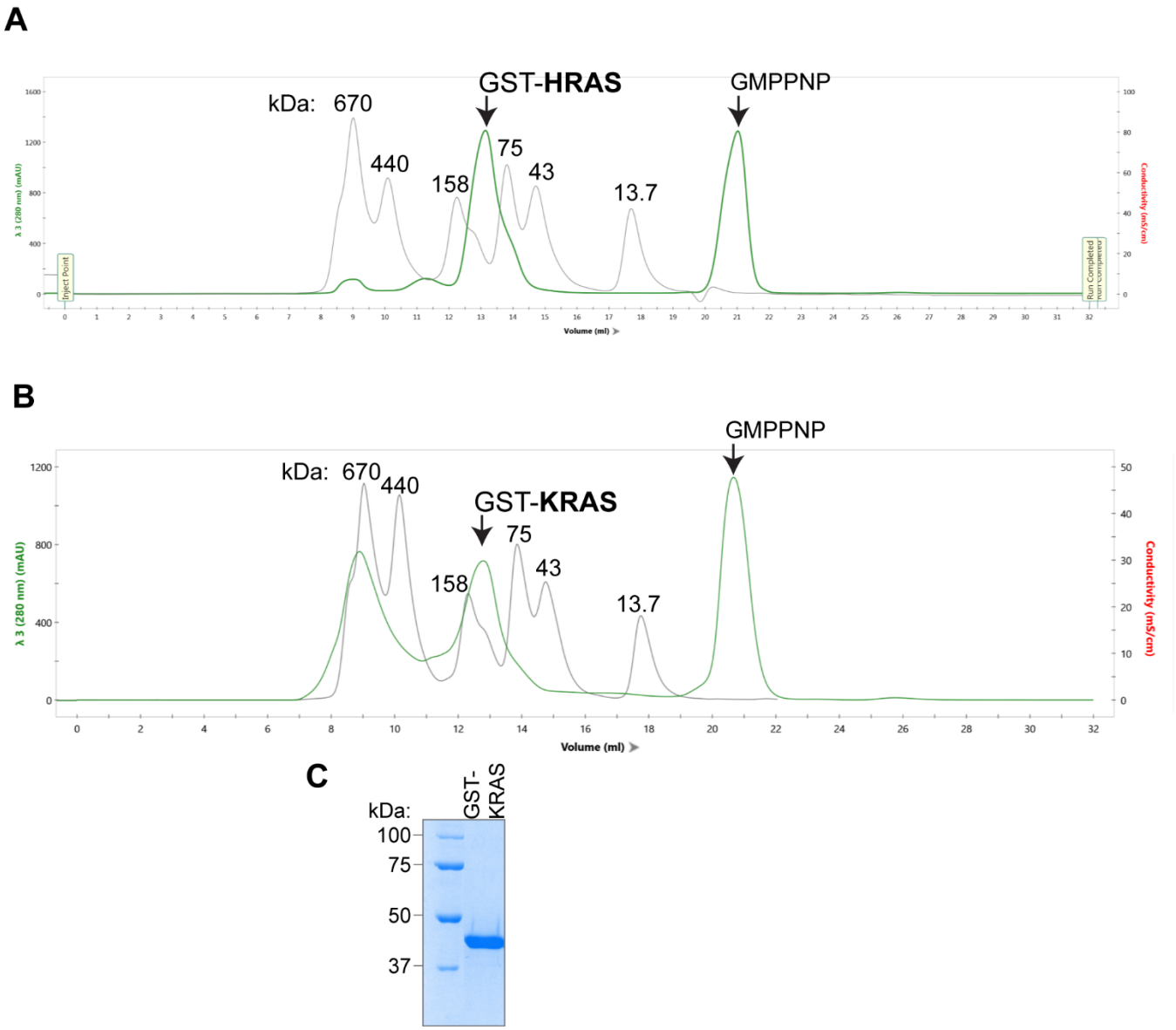

Supplementary Figure 1- SEC of active GST-HRAS and GST-KRAS. (A) GST-HRAS monomer is ~45 kDa and elutes as a dimer at ~90 kDa. HRAS elution profile (green) on a Superdex 200 (Cytiva) overlayed with protein size standard elution profile (gray). (B) GST-KRAS elution profile details the same as GST-HRAS (A). Fractions from ~12-14 mL were collected and concentrated. (C) Coomassie stained gel of GST-KRAS final purification product.

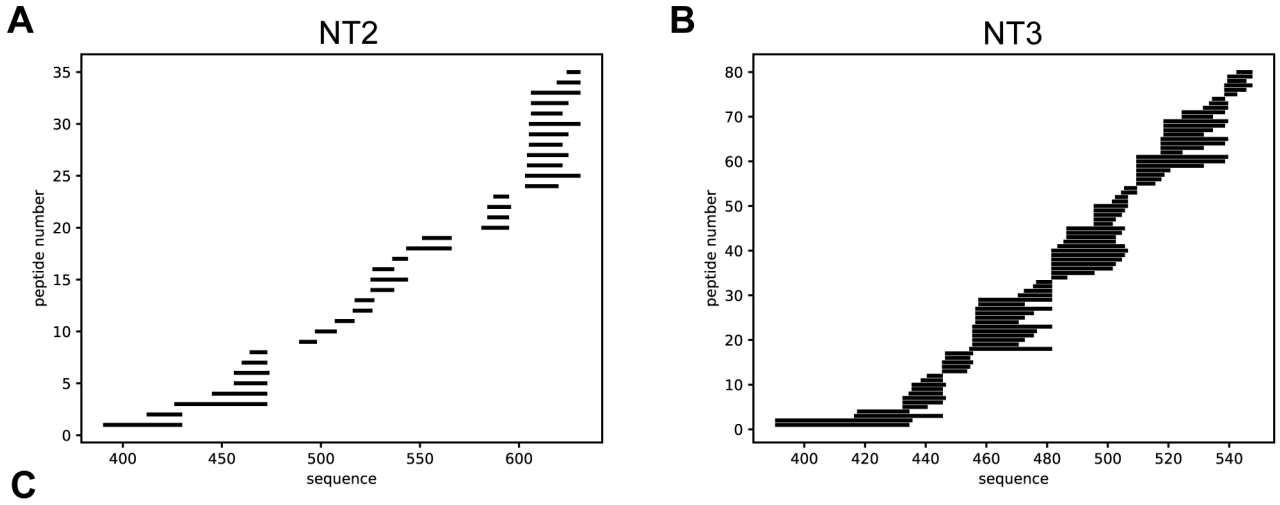

NT2 sequence:

1- MGSSHHHHHHGTKTEEGKLVIWINGDKGYNGLAEVGKKFEKDTGIKVTVEHPDKLEEKFPQ-
VAATGDGPDIIFWAHDRFGGYAQSGLLAEITPDKAFQDKLYPFTWDAVRYNGKLIAYPIAVEALSLIYNKDLLPNP
PKTWEEIPALDKELKAKGKSALMFNLQEPYFTWPLIAADGGYAFKYENGKYDIKDVGVDNAGAKAGLTFLVDLI
KNKHMNADTDYSIAEAAFNKGETAMTINGPWAWSNIDTSKVNYGVTVLPTFKGQPSKPFVGVLSAGINAASPNK
ELAKEFLENYLLTDEGLEAVNKDKPLGAVALKSYEEELAKDPRIAATMENAQKGEIMPNIPQMSAFWYAVRTAVI
NAASGRQTVDEALKDAQTGTDYDIPTTENLYFQGHMASMTGGQQMGRGSAALSGGGGGGAEPGQALFNGDM
EPEAGAGAGAAASSAADPAIPEEVWNIKQMIKLTQEHIEALLDKFGGEHNPPSIYLEAYEEYTSKLDALQQREQQ
LLESLGNGTDFSVSSSASMDTVTSSSSSSLSVLPSSLSVFQNPTDVARSNPKSPQKPIVRVFLPNKQRTVVPARC
GVTVRDSLKKALMMRGLIPECCAVYRIQDGEKKPIGWDTDISWLTGEELHVEVL -632

His/MBP tag
BRAF NT2 (a.a. 1-227)

NT3 sequence:

1- MGSSHHHHHHGTKTEEGKLVIWINGDKGYNGLAEVGKKFEKDTGIKVTVEHPDKLEEKFPQ-
VAATGDGPDIIFWAHDRFGGYAQSGLLAEITPDKAFQDKLYPFTWDAVRYNGKLIAYPIAVEALSLIYNKDLLPNP
PKTWEEIPALDKELKAKGKSALMFNLQEPYFTWPLIAADGGYAFKYENGKYDIKDVGVDNAGAKAGLTFLVDLI
KNKHMNADTDYSIAEAAFNKGETAMTINGPWAWSNIDTSKVNYGVTVLPTFKGQPSKPFVGVLSAGINAASPNK
ELAKEFLENYLLTDEGLEAVNKDKPLGAVALKSYEEELAKDPRIAATMENAQKGEIMPNIPQMSAFWYAVRTAVI
NAASGRQTVDEALKDAQTGTDYDIPTTENLYFQGHMASMTGGQQMGRGSSPQKPIVRVFLPNKQRTVVPARCG
VTVRDSLKKALMMRGLIPECCAVYRIQDGEKKPIGWDTDISWLTGEELHVEVLENVPLTTHNFVRKTFFTLAFCD
FCRKLLFQGFRCQTCGYKFHQRCSTEVPLMCVNYDQLDL -543

His/MBP tag
BRAF NT3 (a.a. 151-288)

Supplementary Figure 2. Stripe Plots for peptides identified in BRAF-NT2 (a) and NT3 (b). Peptide coverage shown begins at the start of BRAF-NT2 or NT3 (not shown: coverage for MBP-tag N-terminal to the BRAF sequence). (C) Protein sequences used in MS analysis.

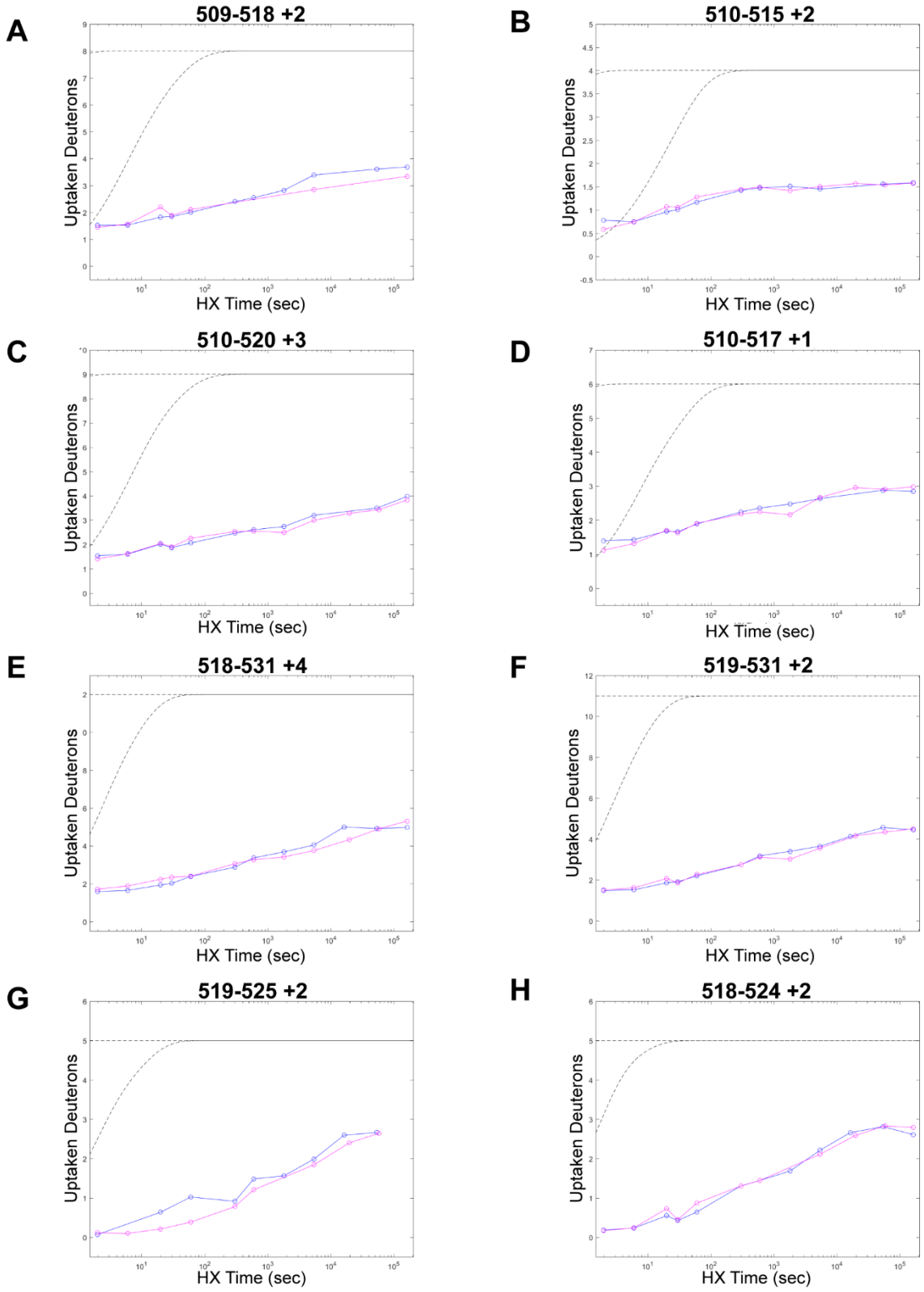

Supplementary Figure 3. Peptides from NT3 in the CRD region. Plots on left represent peptides that could have slowed deuterium uptake. Plots on right represent peptides in the same region

that show essentially no change. Blue= NT3-apo; Magenta= NT3+HRAS. BRAF residues 232-284 (CRD)= peptide residues 491-543.

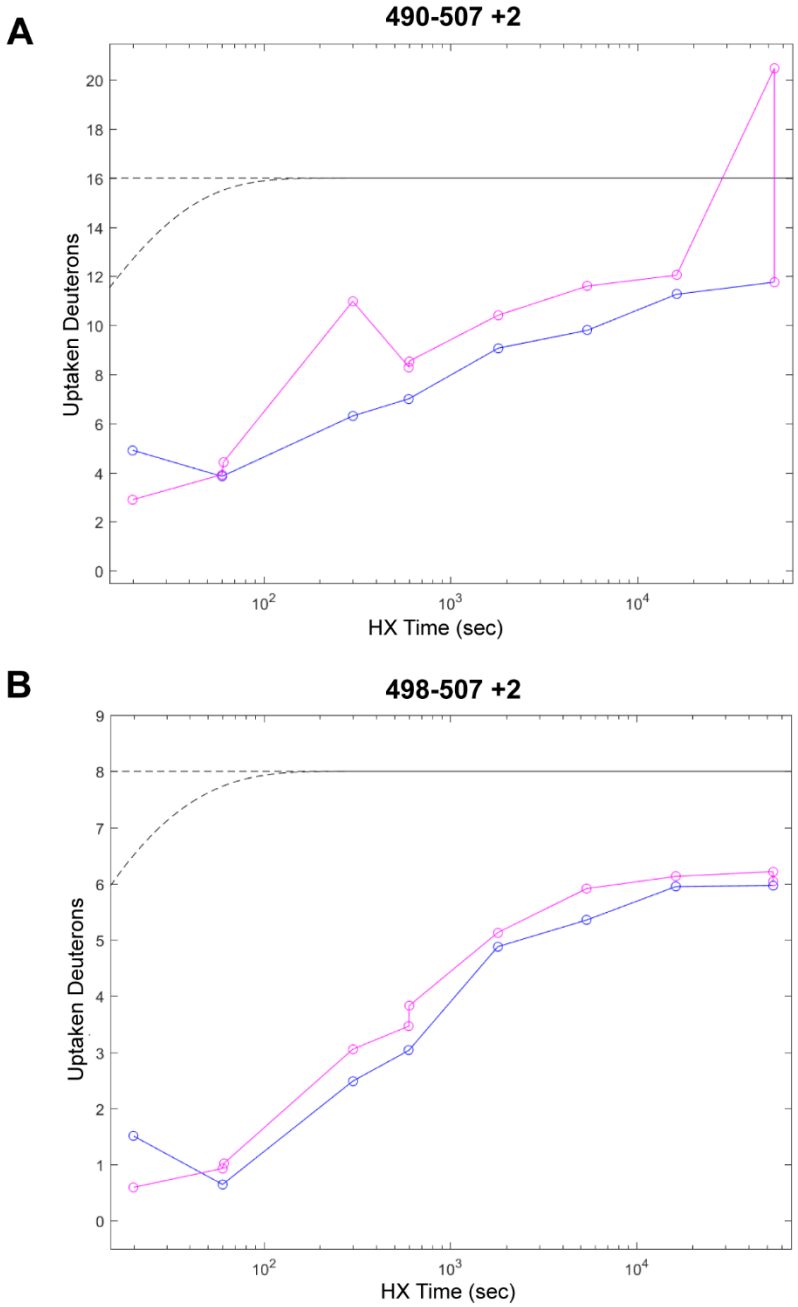

Supplementary Figure 4. Peptides from NT2 in the BSR region (aa. 82-99). Two representative peptide plots that have increased deuterium uptake. Blue= NT2-apo; Magenta= NT2+HRAS. BRAF residues 82-99 correspond with peptide residues 490-507.

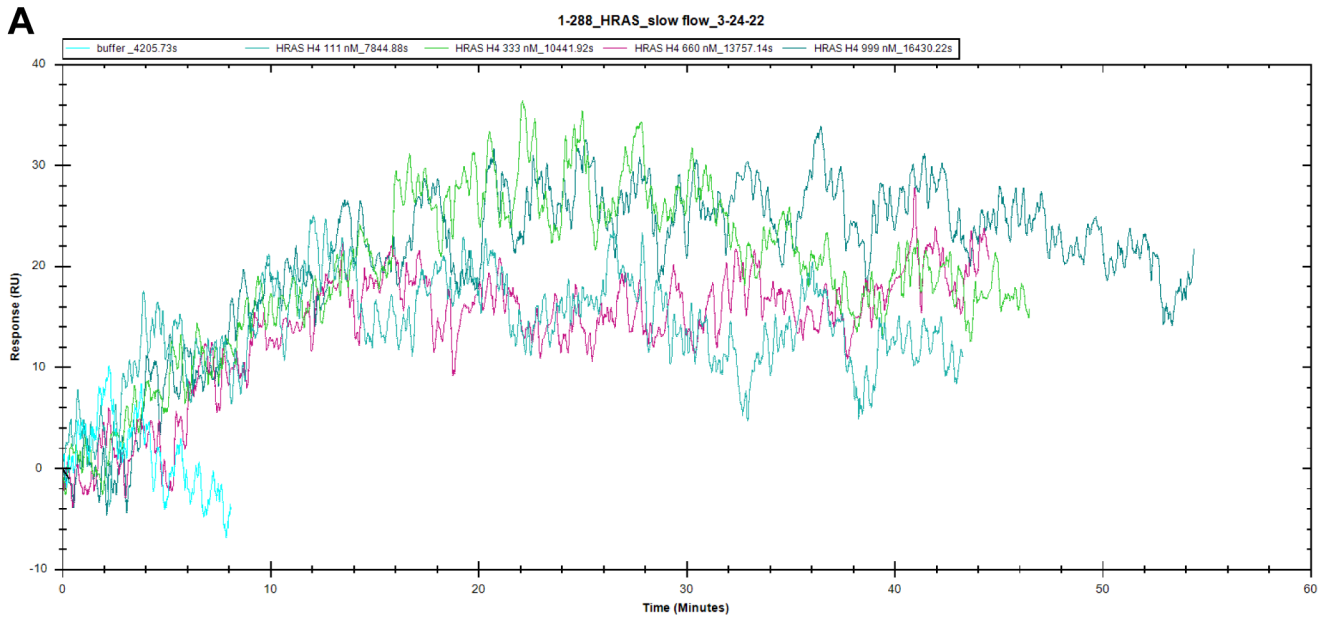

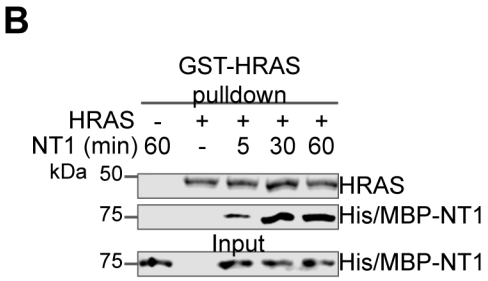

Supplementary Figure 5. HRAS-NT1 SPR shows slow association. (A) OpenSPR injections of HRAS (111, 333, 660, and 999 nM) at 5 ul/min over His/MBP-NT1 immobilized on an NTA sensor. (B) Western blot of GST-HRAS on glutathione resin and NT1 binding through pulldown assay. HRAS was first added to resin for 1 hour. After washing to remove unbound HRAS, NT1 was added in a 1:1 molar ratio and incubated at 4 °C for 5, 30, and 60 minutes. HRAS was probed with GST antibody and NT1 with His antibody.